

Resonant cyclotron scattering in magnetars' emission

N. Rea¹, S. Zane², R. Turolla^{3,2}, M. Lyutikov⁴ and D. Götz⁵

ABSTRACT

We present a systematic application of a resonant cyclotron scattering (RCS) model to a comprehensive set of magnetars, including canonical and transient anomalous X-ray pulsars, and soft gamma repeaters. In this scenario, non-thermal magnetar spectra in the soft X-rays (i.e. below $\sim 10\text{keV}$) result from resonant cyclotron scattering of the thermal surface emission by hot magnetospheric plasma. We find that this model can successfully account for the X-ray emission of magnetars, while using the same number of free parameters than the commonly used empirical blackbody plus power-law model. We find that the entire class of sources is characterized by magnetospheric plasma with similar properties, in particular the optical depth is in a quite narrow range ($\tau_{res} \sim 1-2$). This leads to an estimate of the magnetospheric electron densities at the resonance $n_e \approx 1.5 \times 10^{13} \tau_{res} \text{cm}^{-3}$, which is 3 orders of magnitudes greater than n_{GJ} , the Goldreich-Julian electron density for pulsar magnetospheres. The inferred values of the column densities are also in better agreement with more recent estimates inferred from the fit of single X-ray edges. Considering a large number of datasets allows us to search for correlations between the model parameters either in the time evolution of single sources or in the entire class. Although the treatment of the magnetospheric scattering used here is only approximated, its successful application to all magnetars we considered shows that the RCS model is capable to catch the main features of the spectra observed below $\sim 10\text{keV}$. Future, more detailed modeling of resonant scattering by magnetospheric electrons appears a promising step toward a self-consistent physical interpretation of magnetars soft X-ray emission.

¹University of Amsterdam, Astronomical Institute “Anton Pannekoek”, Kruislaan, 403, 1098 SJ, Amsterdam, The Netherlands; nrea@science.uva.nl

²Mullard Space Science Laboratory, University College London, Holmbury St. Mary, Dorking, Surrey, RH5 6NT, UK

³Department of Physics, University of Padova, Via Marzolo 8, I-35131 Padova, Italy

⁴Department of Physics, Purdue University, 525 Northwestern Avenue, West Lafayette, IN 47907, USA

⁵CEA Saclay, DSM/DAPNIA/Service d’Astrophysique, Gif sur Yvette, France

Subject headings: radiation mechanisms: non-thermal — stars: magnetic fields — stars: neutron — X-rays: individual (4U 0142+614 1RXS J1708-4009, 1E 1841-045, 1E 2259+586, 1E 1048-5937, XTE J1810-197, 1E 1547.0-5408, CXOU J1647-4552, SGR 1806-20, SGR 1900+14)

1. Introduction

The neutron star world, as we knew it until not long ago, appeared mainly populated by radio pulsars (PSRs, about 2000 objects). In the last two decades diverse, puzzling classes of isolated NSs, with properties much at variance with those of canonical PSRs, were discovered: the anomalous X-ray pulsars (AXPs), the soft gamma repeaters (SGRs; Woods & Thompson 2006), the rotating radio transients (RRATs; McLaughlin et al. 2006), and the X-ray dim isolated neutron stars (XDINSs; Haberl 2007). Among these, the AXPs and SGRs are, in some sense, the most peculiar, since they are believed to host ultra-magnetized NSs, with a magnetic field $\approx 10^{14}$ – 10^{15} G, in excess of the critical magnetic field, $B_{crit} \equiv m_e^2 c^3 / (e \hbar) = 4.414 \times 10^{13}$ G, at which the cyclotron energy equals the rest mass energy for an electron (Duncan & Thompson 1992; Thompson & Duncan 1993, 1995, 1996).

The magnetar candidates (about fifteen known objects) are characterized by slow X-ray pulsations ($P \sim 2$ – 12 s) and large spin-down rates ($\dot{P} \sim 10^{-10}$ – 10^{-12} s). A distinctive property is their high persistent X-ray luminosity ($L \approx 10^{34}$ – 10^{36} erg s $^{-1}$), which exceeds the spin-down luminosity typically, by two orders of magnitude. Thus, magnetar X-ray emission can not be explained in terms of rotational energy losses. Measurements of spin periods and period derivatives, assuming that the latter are due to electromagnetic dipolar losses, lend further support to the idea that these objects contain neutron stars endowed with an ultra-strong magnetic field. Although the magnetar model has become increasingly popular, alternative scenarios to explain the enigmatic properties of these sources have been proposed. Among these, models involving accretion from a fossil disk, formed in the supernova event which gave birth to the neutron star, are still largely plausible (e.g. van Paradijs et al. 1995; Chatterjee, Hernquist & Narayan 2000; Perna, Heyl & Hernquist 2000).

Magnetar X-ray emission may be qualitatively separated into two components, a low-energy, $\lesssim 10$ keV, and a high-energy one, $\gtrsim 20$ keV. It is likely that different emission mechanisms are responsible for the two components. The low energy component is typically fit with either a blackbody with a temperature $kT \sim 0.3$ – 0.6 keV and a power-law with a relatively steep photon index, $\Gamma \sim 2$ – 4 , or two blackbodies with $kT_1 \sim 0.3$ keV and $kT_2 \sim 0.7$ keV (see Woods & Thompson 2006 for a review). In a few cases the low-energy component of SGR spectra has been fit with a single power-law, but recent longer observations have

shown that, also for these sources, a blackbody component is required (Mereghetti et al. 2005a). The high-energy component, discovered from four AXPs (Kuiper et al. 2004, 2006) and two SGRs (Mereghetti et al. 2005b; Molkov et al. 2005; Götz et al. 2006) has in general a quite hard spectrum (modeled by a power-law), and accounts for about half of the bolometric luminosity of these sources. This makes it crucial to consider in any spectral modeling the whole 1–200 keV spectrum, where $> 90\%$ of the magnetar emission is concentrated, instead of focussing on the soft X-ray range alone. Furthermore, the discovery of magnetar counterparts in the radio and infrared/optical bands (Camilo et al. 2006; Hulleman et al. 2000) enforced the idea that their multi-wavelength spectral energy distribution is by far more complex than the simple superposition of blackbody (BB) and power-law (PL) distributions.

The purpose of this paper is to provide a physical interpretation for the soft X-ray component ($\lesssim 10$ keV). Our starting point is the work by Thompson, Lyutikov & Kulkarni (2002, TLK in the following), who pointed out that resonant scattering in magnetar magnetospheres may explain the non-thermal spectrum observed below ~ 10 keV. Due to the presence of hot plasma in the neutron star coronae, the thermal emission from the neutron star surface/atmosphere gets distorted through efficient resonant cyclotron scattering. Lyutikov & Gavril (2006) computed, in an approximated and semi-analytical way, the effect of multiple resonant scatterings of soft photons in the magnetosphere, and found that the emerging spectrum is non-thermal, with a shape that may resemble the observed blackbody plus power-law. This model was preliminarily fit to the spectrum of the AXP 1E 1048-5937 (Lyutikov & Gavril 2006), although the magnetospheric parameters were held fixed during the modeling. Rea et al. (2007a,b) implemented in *XSPEC* a more refined version in which also these parameters are minimized during the fit (see §2.2), and successfully modeled a simultaneous *Swift* and *INTEGRAL* observation of 4U 0142+614. In the following, we refer to this *XSPEC* model as the RCS model, where RCS stands for Resonant Cyclotron Scattering. Güver et al. (2007a,b) applied a similar model to two AXPs, taking into account for the fact that the thermal emission from the star surface is not a blackbody if the presence of an atmosphere is accounted for (see also §5). More detailed, fully 3D Monte Carlo simulations of multiple resonant scattering in the star magnetosphere have been very recently presented by Fernandez & Thompson (2007; see also Nobili, Turolla & Zane in preparation) but not yet directly applied to the data yet.

In this paper we present a systematic application of the RCS model to observations of all AXPs and SGRs. We consider the deepest X-ray pointings available up to now for these sources, obtained making use of the large throughput of the *XMM-Newton* satellite. For a subset of sources, which have been detected in the hard X-ray range, we also consider a joint fit with the *INTEGRAL* spectra in order to study systematically the relation between hard and soft X-rays production mechanisms.

The paper is organized as follows. The basic concepts behind the RCS model and its XSPEC implementation are summarized in § 2. In §3 we report the observations and the data analysis. Results of the spectral modeling are presented in §4, and discussed in §5. Conclusions follow.

2. Resonant Cyclotron Scattering

2.1. The model

Before discussing our XSPEC model and the implications of our results, we briefly touch on some properties of the RCS model which directly bear to the physical interpretation of the fitting parameters and their comparison with similar parameters introduced in other theoretical models. The basic idea follows the original suggestion by TLK, who pointed out that a scattering plasma may be supplied to the magnetosphere by plastic deformations of the crust, which twist the external magnetic field and push electric currents into the magnetosphere. The particle density of charge carries required to support these currents may largely exceed the Goldreich-Julian charge density (Goldreich & Julian 1969). Furthermore, it is expected that instabilities heat the plasma.

Following this idea, Lyutikov & Gavril (2006) studied how magnetospheric plasma might distort the thermal X-ray emission emerging from the star surface through efficient resonant cyclotron scattering. If a large volume of the neutron star magnetosphere is filled by a hot plasma, the thermal (or quasi-thermal) cooling radiation emerging from the star surface will experience repeated scatterings at the cyclotron resonance. The efficiency of the process is quantified by the scattering optical depth, τ_{res} , so that the relative fraction of photons that escape without scattering is $\exp(-\tau_{res})$,

$$\tau_{res} = \int \sigma_{res} n_e dl = \tau_0 (1 + \cos^2 \alpha) \quad (1)$$

where

$$\sigma_{res} = \frac{\sigma_T}{4} \frac{(1 + \cos^2 \alpha) \omega^2}{(\omega - \omega_B)^2 + \Gamma^2/4} \quad (2)$$

is the (non-relativistic) cross-section for electron scattering in the magnetized regime, n_e is the electrons number density, α is the angle between the photon propagation direction and the local magnetic field, $\Gamma = 4e^2\omega_B^2/3m_e c^3$ is the natural width of the first cyclotron

harmonic, σ_T is the Thomson scattering cross-section, and

$$\tau_0 = \frac{\pi^2 e^2 n_e r}{3 m_e c \omega_B}. \quad (3)$$

Here r is the radial distance from the center of the star, $\omega_B = eB/m_e c$ is the electron cyclotron frequency, and B is the local value of the magnetic field. At energies corresponding to soft X-ray photons, the resonant scattering optical depth greatly exceeds that for Thomson scattering, $\tau_T \sim n_e \sigma_T r$,

$$\frac{\tau_{res}}{\tau_T} \sim \frac{\pi m_e c^3}{8 e^2 \omega_B} \sim 10^5 \left(\frac{1 \text{ keV}}{\hbar \omega_B} \right). \quad (4)$$

This implies that even a relatively small amount of plasma present in the magnetosphere of the NS may considerably modify the emergent spectrum.

The RCS model developed by Lyutikov & Gavril (2006), and used in this investigation, is based on a simplified, 1D semi-analytical treatment of resonant cyclotron up-scattering of soft thermal photons, under the assumption that scattering occurs in a static, non-relativistic, warm medium and neglecting electron recoil. The latter condition requires $\hbar\omega \ll m_e c^2$. Emission from the neutron star surface is treated assuming a blackbody spectrum, and that seed photons propagate in the radial direction. Since scatterings with the magnetospheric electrons occur in a thin shell of width $H \sim \beta_T r/3 \ll r$ (where β_T is the thermal electron velocity distribution) around the “scattering sphere”, one can treat the scattering region as a plane-parallel slab. Radiation transport is tackled by assuming that photons can only propagate along the slab normal, i.e. either towards or away from the star. Therefore, $\cos \alpha = \pm 1$ in eq. (1) and it is $\tau_{res} = 2\tau_0$. The electron density is assumed to be constant through the slab, while magnetospheric charges are taken to have a top-hat velocity distribution centered at zero and extending up to $\pm\beta_T$. Such a velocity distribution mimics a scenario in which the electron motion is thermal (in 1D because charges stick to the field lines). In this respect, β_T is associated to the mean particle energy and hence to the temperature of the 1D electron plasma. It follows also that the model does not account for the bulk motion of the charges. This is expected since the starting point is not a self-consistent calculation of the currents but a prescription for the charge density. As a consequence, the electron velocity and the optical depth are independant parameters, although in a more detailed treatment this might not be the case (Beloborodov & Thompson 2007).

In the Thomson limit the photon energy is conserved in the electron rest frame, hence the charge thermal motion produces an energy shift in the observer frame. However, since our electron velocity distribution averages to zero, a photon has the same probability to undergo up or down-scattering. Still, a net up-scattering (and in turn the formation of a hard tail in the spectrum) is expected if the magnetic field is inhomogeneous. For a photon

propagating from high to low magnetic fields, multiple resonant cyclotron scattering will, on average, up-scatter in energy the transmitted radiation, while the dispersion in energy decreases with optical depth (Lyutikov & Gavril 2006). Photon boosting by particle thermal motion in Thomson limit occurs due to the spatial variation of the magnetic field and differs qualitatively from the (more familiar) non-resonant Comptonization (Kompaneets 1956). As a result, the emerging spectrum is non-thermal and under certain circumstances can be modeled with two-component spectral models consisting of a blackbody plus a power-law (Lyutikov & Gavril 2006).

2.2. The XSPEC implementation of the RCS model

In order to implement the RCS model in **XSPEC**, we created a grid of spectral models for a set of values of the three model parameters β_T , τ_{res} and T , where T is the temperature of the seed thermal surface radiation, assumed to be a blackbody. The parameter ranges are $0.1 \leq \beta_T \leq 0.5$ (step 0.1), $1 \leq \tau_{res} \leq 10$ (step 1) and $0.1 \text{ keV} \leq T \leq 3 \text{ keV}$ (step 0.05 keV). For each model, the spectrum was computed in the energy range 0.1–12 keV (bin width 0.05 keV). The final **XSPEC atable** spectral model has therefore three parameters, plus the normalization constant, which are simultaneously varied during the spectral fitting following the standard χ^2 minimization technique. In Fig. 1 we show the comparison between a blackbody model and our RCS model. We stress again that our model has the same number of free parameters (four) than the canonical blackbody plus power-law or two blackbody models (β_T , τ_{res} , T , plus the normalization, compared to kT , Γ (or kT_2), plus two normalizations); it has then the same statistical significance. We perform in the following section a quantitative comparison between the RCS model and other models commonly used in the soft X-ray range. However, note that the RCS model is meant to model spectra in the 0.1–12 keV energy range. For all sources with strong emission above ~ 20 keV, the spectrum was modeled by adding to the RCS a power-law meant to reproduce the hard tail (see § 4 for details). This power-law does not have (yet) a clear physical meaning in our treatment, but since it contributes also to the 0.1–12 keV band, our RCS parameters depend on the correct inclusion of this further component.

3. Observations and Data Analysis

Before discussing our data analysis, we would like to outline the choices we made in selecting the datasets to be used in this work. Aim of this paper is to show how the RCS model can account for the X-ray spectra of both steady and variable AXPs and SGRs. Detailed

spectral modeling requires high-quality data and this led us to consider only the highest signal-to-noise ratio datasets available to date for these sources. We selected then only those magnetar candidates having *XMM-Newton* spectra with a number of counts $> 10^5$ and did not include short (< 10 ks) *XMM-Newton* exposures⁶, *Chandra* or *Swift* observations. Fortunately most of the magnetars met the above criterion, but our choice resulted in the exclusion of CXOU J0100-7211, AX J1844-0258, SGR 0526-66, SGR 1627-41 and SGR 1801-23; they are no further considered in the present investigation. The remaining sources are divided into three groups, as follows.

- A set of AXPs which emit in the hard X-ray range, and also happen to be “steady” emitters or showing moderate flux and spectral variability (flux changes $<$ than a factor of 5; with the exception of 1E 2259+586, see also below). These long-term changes are not considered in the following (see § 4.1 for details). This group comprises: 4U 0142+614, 1RXS J1708-4009, 1E 1841-045, and 1E 2259+586. When more than one *XMM-Newton* observation was available, we chose the dataset with the longest exposure time and less affected by background flares.
- A set of “transient” AXPs (often labelled TAXPs), which includes XTE J1810-197, 1E 1547.0-5408, and CXOU J1647-4552. To these we add 1E 1048-5937, in the light of the recent detection of large outbursts from this source (Mereghetti et al. 2004; Gavriil et al. 2006; Tam et al. 2007; Campana & Israel 2007), and of its spectral similarities with canonical TAXPs. In order to follow the spectral evolution without being encumbered with unnecessary details, we selected only three *XMM-Newton* spectra for each source, also when more observations were available (e.g. for 1E 1048-5937, XTE J1810-197, and SGR 1806-20). The three chosen datasets correspond to the two most diverse spectra and to an “intermediate” state.
- A set of SGRs, which comprises SGR 1806-20 (three observations covering epochs before and after the giant flare of 2004 December 27), and SGR 1900+14.

For all the sources in the first group (except 1E 2259+586) and for SGR 1900+14 we also considered *INTEGRAL* data. Despite *INTEGRAL* and *XMM-Newton* observations were not always simultaneous, the absence of large spectral variability in these sources justifies our choice. In particular, for SGR 1900+14 care has been taken to select data relative to periods in which the source was relatively steady. Although AXP 1E 2259+586 and SGR 1806-20 have been also detected above 20 keV (Kuiper et al. 2006; Mereghetti et al. 2005b; Molkov et

⁶Except for 1E 1841-045, for which only a single short *XMM-Newton* observation is available.

al. 2005), the *INTEGRAL* X-ray counterpart of the former is too faint to extract a reliable spectrum, while the highly variable hard and soft X-ray spectrum of the latter, together with the non simultaneity of the *XMM-Newton* and *INTEGRAL* observations, would make any attempt to model its 1–200 keV spectral energy distribution meaningless (see also Esposito et al. 2007).

The following subsections provide some details on the observations and data analysis; a comprehensive log, with the exposure times and epochs of each observation, is provided in Tab. 1.

3.1. XMM-Newton: soft X-rays

All soft X-ray spectra were collected by the *XMM-Newton* EPIC-pn instrument (Jansen et al. 2001; Strüder et al. 2001), which has the largest sensitivity in the 1-10 keV band. In order to have a homogeneous sample of spectra, we re-analysed all the data using the latest SAS release 7.1.0. We employed the most updated calibration files available at the time the reduction was performed (August 2007). Standard data screening criteria (e.g. cleaning for background flares) were applied in the extraction of scientific products. We used FLAG= 0 and PATTERN between 0 – 4 (i.e. single and double events) for all the spectra. We have checked that spectra generated with only single events (i.e. PATTERN= 0) agreed (apart from normalisation factors) with those generated from single and double events. All the EPIC-pn spectra were rebinned before fitting, using at least 30 counts per bin and not oversampling the resolution by more than a factor of 3 (see Rea et al. 2005, 2007c for further details on *XMM-Newton* data analysis and reduction).

3.2. INTEGRAL: hard X-rays

In order to take into account in our spectral modeling for the contribution of the hard X-ray emission of 4U 0142+614, 1RXS J1708-4009, 1E 1841-045 and SGR 1900+14, we used the hard X-ray spectra taken with the *INTEGRAL* satellite. We selected and analyzed all publicly available IBIS (Ubertini et al. 2003) pointings, making use of ISGRI (Lebrun et al. 2003), the IBIS low energy detector array working in the 15 keV–1 MeV energy range. Data were collected for all pointings within 12° from the direction of each source, for a total 2544, 1351, 1894 and 1535 pointing of 2-3 ks each, for the three AXPs and the SGR, respectively. Given the low hard X-ray flux of these sources, we added all the data in order to have statistically significant detections.

We processed the data using the Offline Scientific Analysis (OSA) software provided by the *INTEGRAL* Science Data Centre (ISDC) v6.0. We produced the sky images of each pointing in 10 energy bands between 20 and 300 keV, and added them in order to produce a mosaicked image. Due to the faintness of the sources we could not derive their spectra from the individual pointings. So following e.g. Götz et al. (2007), we used the count rates of the mosaicked images to build time averaged the spectrum of each source.

4. Spectral Analysis and Results

All the fits have been performed using *XSPEC* version 11.3 and 12.0, for a consistency check. A 2% systematic error was added to the data to partially account for uncertainties in instrumental calibrations. A constant function has been fitted when using both *XMM-Newton* and *INTEGRAL* data to account for inter-calibration uncertainties (the values of the constant in the Tables are relative to *XMM-Newton* set to unity). The 0.5–1 keV energy range was excluded from our spectral fitting because: *i*) this is the band where most of the calibration issues lay (Haberl et al. 2004), and *ii*) emission in this energy range is mostly affected by interstellar absorption. Given the high column density of all magnetars, and the large uncertainties in the abundances (probably not even solar) in their directions, this may lead to spurious features. We checked that for all our targets, the values of N_H derived fitting the 1–10 keV EPIC-pn spectra, are consistent (within 1σ) with those obtained using the 0.5–10 keV range in the same data set. We notice that the absorption derived here for the canonical model is, on average, slightly higher than that reported in the literature for the same model. This is due to our choice of using the more updated solar abundances by Lodders (2003), instead of the older ones from Anders & Grevesse (1989). This does not affect the other spectral parameters, which are in fact consistent with those previously published for the same data sets.

We caveat that no attempt has been made here to distinguish the pulsed from the non-pulsed emission of these objects, and to model the spectral variability with phase observed in most of these sources. This will be the subject of a future investigation.

4.1. AXPs: the hard X-ray emitters

In this section we first consider the AXPs with detected hard X-ray emission, which also coincides with the marginally variable AXPs, with the exception of 1E 2259+586 (Kaspi et al. 2003; Woods et al. 2004; see below). We remind that, strictly speaking, these hard

emitting AXPs are not “steady” X-ray emitters. Subtle flux and spectral variability was discovered in 1RXS J1708-4009 and 4U 0142+614. In particular, 1RXS J1708-4009 showed a long term, correlated intensity-hardness variability (both in the soft and hard X-rays), most probably related to its glitching activity (Rea et al. 2005; Campana et al. 2007; Götz et al. 2007; Israel et al. 2007a; Dib et al. 2007a). 4U 0142+614 showed a flux increase of $\sim 10\%$ (also correlated with a spectral hardening) following the discovery of its bursting activity (Dib et al. 2007b; Gonzalez et al. 2007). Furthermore, thanks to a large *RXTE* monitoring campaign, long-term spin period variations and glitches were discovered in 4U 0142+614 1RXS J1708-4009, and 1E 1841-045, i.e. the three AXPs which are the brightest both in the soft and hard X-ray bands (Gavril & Kaspi 2002; Dall’Osso et al. 2003; Dib et al. 2007a; Israel et al. 2007a).

Since these flux variations are rather small, we have chosen to model only the *XMM-Newton* observation closest to the *INTEGRAL* one (for 1RXS J1708-4009 only one *XMM-Newton* observation is available though). Our results from the spectral modeling of the 1–200 keV spectrum of 4U 0142+614 1RXS J1708-4009, and 1E 1841-045 are summarized in Table 6 and shown in Fig. 2.

The case of 1E 2259+586 is rather different: it showed a large outburst (more than one order of magnitude flux increase) detected by *RXTE*, during which also bursting activity was detected (Kaspi et al. 2003). However, in the *XMM-Newton* observations pre and post outburst, the source showed fluxes which differ only by a factor of 3 (Woods et al. 2004). Furthermore, it was observed to emit up to ~ 30 keV by the HEXTE instrument on board of *RXTE* (Kuiper et al. 2006) and by *INTEGRAL*, but unfortunately it is too faint in the latter to extract a spectrum out of it. We then decided to model only the deepest *XMM-Newton* observation taking into account of its >10 keV component by adding a power-law with photon index fixed at the HEXTE value (Kuiper et al. 2006). This is because sizable residuals are present at the highest energies when the *XMM-Newton* spectrum is modeled either with the canonical BB+PL or the RCS model. A satisfactory fit requires, in both cases, the addition of a hard X-ray power-law component (see also Table 3 and Fig. 3).

Summarizing, the only source that can be considered a genuine “steady” X-ray emitter, among the AXPs with hard X-ray emission is 1E 1841-045. It is interesting to note that this is also the only AXPs for which a blackbody plus a single power-law reproduces well the entire 1-200 keV spectrum, while for the other hard X-ray emitting AXPs two power-laws are required. In this respect, the spectral distribution of 1E 1841-045 resembles the one of the SGRs (see also §5).

In all cases we found that N_H , as derived from the RCS model, is lower than that inferred from the canonical BB+2PL (or BB+PL in the case of 1E 1841-045) fit, and consistent

with what derived from fitting the single X-ray edges of 4U 0142+614, 1E 2259+586, and 1RXS J1708-4009 (Durant & van Kerkwijk 2006). This is not surprising, since the power-law usually fitted to magnetar spectra in the soft X-ray range is well known to cause an overestimate of the column density. The surface temperature we derived fitting the RCS model is systematically lower than the corresponding BB temperature in the BB+2PL or BB+PL models, and is consistent with being the same (~ 0.34 keV) in all sources. On the other hand the thermal electron velocity and the optical depth are in the ranges 0.2 – $0.4c$ and 1.2 – 1.7 , respectively. Concerning the hard X-ray power-law, we find that the photon index is, within the errors, the same when fitting the RCS or the BB+2PL or BB+PL models (except for 1E 2259+586 where it was kept fixed), while the hard PL normalization is always larger in the RCS case. Both the soft and the hard X-ray fluxes of all these AXPs derived from the RCS fitting are consistent with those implied by the canonical BB+2PL fitting.

4.2. AXPs: the “transients”

The “transient” nature of AXPs has been discovered only very recently, when an increase in the X-ray flux by a factor ~ 100 over the value measured a few years before was observed in XTE J1810-197 (Ibrahim et al. 2004; Gotthelf et al. 2004). Later on, new TAXPs have been observed showing large flux and spectral variations, e.g. CXOU J1647-4552 (Muno et al. 2007) and 1E 1547.0-5408 (Gelfand & Gaensler 2007; Camilo et al. 2007a; Halpern et al. 2007). Very intriguing is the discovery of pulsed radio emission correlated with the outbursts of XTE J1810-197 and 1E 1547.0-5408 (Camilo et al. 2006, 2007a), while so far only upper limits have been set on the radio emission from CXOU J1647-4552, 1E 1048-5937 and other AXPs (Burgay et al. 2006, 2007; Camilo et al. 2007b).

It is not clear whether AXPs and TAXPs are indeed two distinct groups of sources. During the past few years it has become increasingly evident that flux variations of various intensities also occur in “steady” AXPs, possibly related to their bursting and glitching activity (see §4.1). This has been observed in 1E 2259+586 (Kaspi et al. 2003), 4U 0142+614 (Dib et al. 2007b, Gonzalez et al. 2007) and 1RXS J1708-4009 (Rea et al. 2007; Campana et al. 2007). Furthermore, bursts have been observed also during the outbursts of the TAxP XTE J1810-197 (Woods et al. 2005) and CXOU J1647-4552 (Muno et al. 2007), the latter also showing a large glitch (Israel et al. 2007b). However, in this paper we maintain the distinction between TAXPs and AXPs, partly for historical reasons, and partly because the two classes may indeed have different spectral properties, with the TAXPs being characterized by much softer X-ray spectra, and by the lack, so far, of detection at energies > 10 keV.

The results of the TAXPs spectral modeling are summarized in Tables 6, 6, 6, 7, and

shown in Figs. 4, 5, 6, 7. Again, N_H derived with the RCS model is lower than (or consistent with) that inferred from the canonical BB+BB fitting for XTE J1810-197, CXOU J1647-4552, and 1E 1547.0-5408, and significantly lower in the case of the BB+PL model applied to 1E 1048-5937 (and consistent with that derived by Durant & van Kerkwijk 2006). We also found that the RCS model can easily account for all the spectral and intensity changes in the TAXPs. With the exception of XTE J1810-197, the surface temperature we derive for all the TAXPs is lower than, or consistent with, that of the blackbody in the canonical model (for the BB+BB model, we refer to the BB with the lowest temperature). However, considering only the RCS model, it is evident for all three TAXPs that the outburst state has a high surface temperature which cools down during the decay. Also for these transient sources, the fluxes implied by the canonical and the RCS model are consistent.

4.3. SGRs

Finally, we consider the 1–10 keV and 1–200 keV emission of SGR 1806-20 (see Table 6 and Fig. 8) and SGR 1900+14 (see Table 9 and Fig. 9). It has been already noticed that the hard X-ray emission of SGRs is quite different from that of AXPs (see §4.1). In fact, with the exception of 1E 1841-045, AXPs spectra show a clear turnover between 10 and 20 keV (see Fig. 2) and their fit requires an additional spectral component. Instead, SGRs hard X-ray emission seems the natural continuation of the non-thermal component which is dominant in the 1–10 keV energy range. This is why we can use a BB (or RCS) plus a single power-law in the entire 1–200 keV range for SGR 1900+14, while for the hard X-ray emitting AXPs we were forced to add a second power-law to the canonical model.

Similar considerations hold for SGR 1806-20, in which case we model the 1–10 keV emission by adding a power-law component which is intended to account for the contribution of the hard X-ray emission in the soft X-ray range. For the latter SGR we modeled three X-ray observations taken before and after the Giant Flare of 2004 December 27 (Hurley et al. 2005; Palmer et al. 2005). We found that the N_H value is consistent between the BB+PL and the RCS+PL models, and the power-law contribution and the photon index vary among the three spectra in a similar fashion for the two models. What is interesting is the fact that when using a BB+PL model the spectral changes are accounted for by a variable BB temperature, while, in the RCS+PL model the surface temperature remains constant within the errors, and the spectral variability is accounted for only by changes in the parameters describing the magnetospheric currents, with β_T and τ_{res} varying in the ranges 0.11–0.45 and in the 1.0–2.1, respectively.

In the SGR 1900+14 1–200 keV spectrum, we found consistent N_H and spectral index

values between the BB+PL and RCS+PL models, and a RCS surface temperature significantly lower than the corresponding BB temperature. In all the SGR observations, the derived fluxes are consistent among the two models.

5. Discussion

Before discussing our results and the physics we can derive from our RCS model, we would like to stress once again that the RCS model involves a number of simplifications (see §2.1). One is the assumption of a single temperature surface emission. Current-carrying charges will hit and heat the star surface, generally inhomogeneously (TLK). In addition, the emission emerging from the surface is likely to be non-Plankian. While the presence of an atmosphere on top the crust of a magnetar remains a possibility (see Güver et al. 2007a,b), its properties, then, are likely different from those of a standard (in radiative and hydrostatic equilibrium) atmosphere on, e.g., a canonical isolated cooling neutron star (see e.g. Ho & Lai 2003; van Adelsberg & Lai 2006). The extreme field and (relatively) low surface temperature ($\lesssim 0.5$ keV) of magnetar candidates may also be suggestive of a condensed surface, at least if the chemical composition is mainly Fe (see Turolla, Zane & Drake 2004). In the light of these considerations, and in the absence of a detailed model for the surface emission, and for the atmosphere of a strongly magnetized NSs constantly hit by returning currents, we restricted ourself to a blackbody approximation for the seed thermal photons.

Despite (or merit) of these simplifications, we find that the RCS model can describe the whole set of magnetar spectra we have considered, including the TAXPs variability, by using only three free parameters (plus a normalization factor), the same number of degree of freedom required by the canonical blackbody plus power-law fitting.

5.1. Magnetar magnetospheric properties

One of the most interesting outcomes of our analysis is that in all sources, steady and variable ones, the value of τ_{res} is in a quite narrow range, $\tau_{res} \sim 1$ –2, although our grid of tabulated models allows for a much larger range of optical depths ($1 \leq \tau_{res} \leq 10$). This suggests that the entire class of sources are characterized by similar properties of scattering electrons, their density and their (thermal) velocity spread. An optical depth $\tau_0 = \tau_{res}/2$ requires a particle density n_e (see eq. [3])

$$\tau_0 \approx 1.8 \times 10^{-20} n_e r_{sc} \left(\frac{1 \text{ keV}}{\hbar \omega_B} \right), \quad (5)$$

where r_{sc} is the radius of the scattering sphere

$$r_{sc} \approx 8R_{NS} \left(\frac{B}{B_{crit}} \right)^{1/3} \left(\frac{1 \text{ keV}}{\hbar\omega_B} \right)^{1/3}, \quad (6)$$

R_{NS} is the neutron star radius and $B_{crit} \approx 4.4 \times 10^{13}$ G is the quantum critical field. By taking a typical photon energy of ~ 1 keV, $R_{NS} \sim 10^6$ cm and $B \sim 10B_{crit}$, we get $n_e \approx 1.5 \times 10^{13} \tau_{res} \text{ cm}^{-3}$. This is several orders of magnitude larger than the Goldreich-Julian density (Goldreich & Julian 1969) at the same distance, $n_{GJ} \approx n_e \pi r_{sc} / (3\tau_{res} R_{lc}) \sim 2 \times 10^{10} \text{ cm}^{-3}$ (where R_{lc} is the light cylinder radius and we took $P \sim 10$ s). While the charge density is large when compared with the minimal Goldreich-Julian density, it is still very small in order to provide a sizable optical depth to non-resonant Thomson scattering. Only the resonant cyclotron scattering makes an efficient photon boosting possible.

Our present model does not include a proper treatment of magnetospheric currents, so that τ_{res} is a free parameter related to the electron density. Nevertheless, it is useful to compare the values of the optical depth inferred here to those expected when a current flow arises because a steady twist is implanted in the star magnetosphere, as in the case investigated by TLK under the assumption of axisymmetry and self-similarity. If the scattering particles participate to a collective motion (bulk velocity β_{bulk}), the efficiency of the scattering process is related to $\tau_{res}\beta_{bulk}$ (e.g. Nobili, Turolla & Zampieri 1993). This quantity is shown as a function of the magnetic colatitude in Fig. 5 of TLK for different values of the twist angle, $\Delta\phi_{N-S}$. By assuming $\beta_{bulk} = 1$ and integrating over the angle, we get the average value of the scattering depth as a function of $\Delta\phi_{N-S}$, which is shown in Fig. 10. The curves corresponding to a different value of β_{bulk} can be obtained simply by reading the quantity shown in Fig. 10 as $\tau_{res}\beta_{bulk}$ and by rescaling the y -axis. As we can see, a value of $\tau_{res} \sim 1$ is only compatible with very large values of the twist angle (i.e. $\Delta\phi_{N-S} > 3$), while typical values of $\tau_{res} \sim 2$, as those obtained from some of our fits, require $\beta_{bulk} \lesssim 0.5$ to be compatible with $\Delta\phi_{N-S} \sim 3$ (the smaller is β_{bulk} , the smaller is the value of the twist angle). This is consistent with the fact that the RCS model has been computed under the assumption of vanishing bulk velocity for the magnetospheric currents, and it is compatible with TLK model only when in the latter it is $\beta_{bulk} \ll 1$.

5.2. Comparison between AXPs and SGRs

In the last few years the detection of bursts from AXPs (Gavriil et al. 2002; Kaspi et al. 2003) strengthened their connection with SGRs. However, the former behave differently in many respects. Below ~ 4 keV, the SGRs emission can be described either by a blackbody or an RCS component. At higher energies though (> 4 keV), their spectra require the addition

of a power-law component, which well describes the spectrum until ~ 200 keV. The non-thermal component dominates their spectra to the point that the choice of a blackbody or the RCS model at lower energies does not affect the value of the hard X-ray power-law index, $\Gamma \sim 1.5$ (see e.g. Fig. 9), nor the energy at which this component starts to dominate the spectrum. SGRs spectra are then strongly non-thermally dominated in the 4–200 keV range.

The case of the AXPs is different (with the exception of 1E 1841-045 see below). These sources show a more complex spectrum, with an evident non-thermal component below ~ 10 keV, apparently different from that observed at higher energies. For the AXPs detected at energies >20 keV, the spectrum can be described by a RCS component until 5–8 keV, above which the non-thermal hard X-ray component becomes important, and (e.g. for 1RXS J1708-4009 and 4U 0142+614) dominates until ~ 200 keV. In the case of the canonical BB+2PL model instead, the non-thermal component responsible for the hard X-ray part of the spectrum starts to dominate only above ~ 10 keV (see e.g. Figs. 2 and 3). This is important, because the measurement of a down-break of the hard X-ray power-law has remarkable physical implications and may prove useful in constraining the physical parameters of the model for the hard X-ray emission (Esposito et al. 2007). It is worth noting that the photon index of the hard X-ray component in AXPs does not strongly depend on the modeling of the spectrum below 10 keV, while, its normalization and, as a consequence, the value at which the hard tail starts to dominate the spectrum, do.

In this picture 1E 1841-045 seems an exception. From the spectral point of 1E 1841-045 appears as the more SGR-like among the AXPs. Its multi-band spectrum can be well fitted by a BB+PL or RCS+PL model, with parameters very similar to SGRs (compare Figs. 9, 2 and Tables 9, 2). This may suggest that this source is a potential transition object between the two classes. However, at variance with the SGRs this is one of the least active bursters among AXPs.

The fact that hard X-ray spectra detected from AXPs are much flatter than those of SGRs may also suggest a possible difference in the physical mechanism that powers the hard tail in the two classes of sources. Within the magnetar scenario, Thompson & Beloborodov (2005) discussed how soft γ -rays may be produced in a twisted magnetosphere, proposing two different pictures: either thermal bremsstrahlung emission from the surface region heated by returning currents, or synchrotron emission from pairs created higher up (~ 100 km) in the magnetosphere. Moreover, a third scenario involving resonant magnetic Compton up-scattering of soft X-ray photons by a non-thermal population of highly relativistic electrons has been proposed by Baring & Harding (2007). It is interesting to note that 3D Monte Carlo simulations (Fernandez & Thompson 2007; Nobili, Turolla & Zane in preparation) show that

multiple peaks may appear in the spectrum. In particular, in the model by Nobili, Turolla & Zane (in preparation), a second “hump” may be present when up-scattering is so efficient that photons start to fill the Wien peak at the typical energy of the scattering electrons. The change in the spectral slope may be due, in this scenario, to the peculiar, “double-humped” shape of the continuum. The precise localization of the down-break is therefore of great potential importance and might provide useful information on the underlying physical mechanism responsible for the hard emission.

The RCS model applied to the evolution of the outbursts of the TAXPs known up to now shows how the outburst may results from a heating of the NS surface, which slowly cools in a timescale of months/years. AXPs outbursts are thought to be caused by large scale rearrangement of the surface/magnetospheric field, either accompanied or triggered by fracturing of the NS crust. It is worth noticing that from our modeling we find that the magnetospheric characteristics does not change much during the outburst, or least not as much as the surface temperature.

5.3. Correlations

The quite large number of observations we analyzed (both relative to different sources and to single sources at different epochs) allows to search for possible correlations among the various quantities, both in the entire sample, i.e. looking at the population of magnetar candidates at large, and in the time evolution of a single source.

Fig. 6 summarizes the results of our spectral fits. The various panels show how the three model parameters (T , τ_{res} and β_T) are related to the (absorbed) X-ray luminosity in the 1–10 keV band ($L_{1-10\text{ keV}}$) and to the magnetic field B . The latter is derived from P and \dot{P} assuming that the magnetic field is a core-centered dipole and spin-down is produced by magneto-rotational braking, therefore the corresponding plots must be regarded only in view of a comparison with this standard derivation.

Eye inspection of the panels in Fig. 6 does not reveal any obvious correlation for the entire set of observations, with the exception of a possible link between $L_{1-10\text{ keV}}$ and the surface temperature. To verify this, we have run a Spearman rank test and found a positive correlation (deviation from the null hypothesis at about the 93% confidence level) between $L_{1-10\text{ keV}}$ and T . A second correlation, although at a reduced confidence level ($\sim 83\%$), exists between the luminosity and the optical depth. No correlations with a significance level above $\sim 60\%$ were found in all the other cases. The increase in the surface temperature with increasing luminosity in the RCS model is quite expected and reflects the fact that a higher

T produces more thermal photons. This, in turn, enhances the soft, thermal component of the spectrum, and, at the same time, provides more seeds for resonant up-scattering. The correlation between τ_{res} , which actually controls together with β_T the scattering efficiency, and $L_{1-10\text{ keV}}$ indicates that at higher fluxes the contribution from the non-thermal, scattering tail increases. Sources with higher luminosities seem then to be characterized by both a higher surface temperature (which translates into more thermal photons) and a more efficient energy transfer from the magnetospheric particles to the radiation field. The latter effect occurs primarily because of the larger particle density, while the electron typical velocity (being not correlated with $L_{1-10\text{ keV}}$) is more or less the same. This is in agreement with the correlation found by Marsden & White (2001) in AXPs and SGRs between the spectral index and the flux (harder spectra at higher fluxes) and also with the results of Monte Carlo simulations of radiative transfer in the twisted magnetosphere model (Fernandez & Thompson 2007; Nobili, Turolla & Zane in preparation). In this picture an increase of the twist angle corresponds to larger currents and, for a constant particle bulk velocity, to larger depths. The higher scattering efficiency produces then a flatter power-law tail.

The same trend discussed above is found restricting to observations of the same source at different epochs as far as the correlation between $L_{1-10\text{ keV}}$ and T is concerned. An increase of the surface temperature with increasing luminosity is clearly present in all the variable sources we examined, i.e. 1E 1048-5937, XTE J1810-197, 1E 1547.0-5408, CXOU J1647-4552 and SGR 1806-20. The situation is not so clear, instead, for the variations of τ_{res} and β_T with the luminosity. Actually, CXOU J1647-4552 and XTE J1810-197 are the only sources for which there is a simultaneous increase or decrease of both τ_{res} and β_T , while increasing the luminosity. In particular, the behaviour of XTE J1810-197 is somehow peculiar, since it means that at larger fluxes the efficiency of RCS drops, which mirrors a more thermal spectrum; in all the other cases at least one of the two parameters τ_{res} or β_T , increases, and this may be enough to guarantee that the spectrum hardens at larger luminosities.

6. Conclusion

In this paper we showed that the soft X-ray emission of magnetars can be explained by resonant cyclotron scattering of their thermal surface emission by a cloud of hot magnetospheric electrons. This model satisfactorily reproduces the spectral shape of all magnetars soft X-ray emission, using the same number of free parameters than the canonical blackbody plus power-law model, although based on a number of simplifying assumptions. This means that the RCS model not only catches the main features of the thermal and non-thermal components observed in these sources below $\sim 10\text{ keV}$, but also successfully provides a

quantitative interpretation. Furthermore, we found that the 1–10 keV luminosity of magnetars correlates with their surface temperature and, at lower confidence level, magnetospheric optical depth. For most of the variable sources similar trends have been found when analyzing different states of the same source.

This work represents the first omni-comprehensive attempt to a physical interpretation of magnetars emission below ~ 10 keV, and to infer some physical values from their spectra. Future refinements of the RCS model from a 1-D analytical model toward a Monte Carlo based code (as the more advanced codes developed by Fernandez & Thompson 2007 and Nobili, Turolla & Zane in preparation), eventually applied to the detailed spectra that *XEUS* and/or *Con-X* will possibly make available in the near future, appear a promising step toward the complete understanding of the physics behind magnetars soft X-ray emission.

We acknowledge Valentina Bianchin and Gavin Ramsay for their help in building the XSPEC RCS model, and Fotis Gavriil for kindly allowing us to look into his preliminary model. Furthermore, we thank Gianluca Israel and Andrea Tiengo for useful discussions and comments on a preliminary draft. NR acknowledges the warm hospitality of the Mullard Space Science Laboratory, where this work was started, and is supported by an NWO Veni Fellowship. SZ acknowledges STFC for support through an Advanced Fellowship. DG acknowledges the French Space Agency (CNES) for financial support. This paper is based on observations obtained with *XMM-Newton* and *INTEGRAL*, which are both ESA science missions with instruments and contributions directly funded by ESA Member States and the USA (through NASA). The XSPEC RCS model is available upon request.

REFERENCES

- Anders, E. & Grevesse, N., 1989, *Geochimica & Cosmochimica Acta* 53, 197
- Beloborodov, A. M. & Thompson, C. 2007, *ApJ*, 657, 967
- Burgay, M., Rea, N., Israel, G. L., Possenti, A., Burderi, L., di Salvo, T., D’Amico, N., Stella, L. 2006, *MNRAS*, 372, 410
- Burgay, M., Rea, N., Israel, G. L., Possenti, A. 2007, *ATel*, # 903
- Campana, S., Rea, N., Israel, G. L., Turolla, R., Zane, S., 2007, *A&A*, 463, 1047
- Chatterjee, P., Hernquist, L., & Narayan, R., 2000, *ApJ*, 534, 373

- Camilo, F., Ransom, S. M., Halpern, J. P., Reynolds, J., Helfand, D. J.; Zimmerman, N., Sarkissian, J. 2006, *Nature*, 442, 892
- Camilo, F., Ransom, S. M., Halpern, J. P., Reynolds, J. 2007a, *ApJ*, 666, L93
- Camilo, F. & Reynolds, J., 2007b, *ATel* # 1056
- Dall’Osso, S., Israel, G.L., Stella, L., Possenti, A., & Perozzi, E. 2003, *ApJ*, 499, 485
- Dib, R., Kaspi, V. M., Gavriil, F. 2007a, *ApJ* in press, arXiv0706.4156
- Dib, R., Kaspi, V. M., Gavriil, F. P., Woods, P. M. 2007b, *ATel* # 104
- Duncan, R.C., & Thompson, C. 1992, *ApJ*, 392, L9
- Durant, M., & van Kerkwijk, M. H., 2006, *ApJ*, 650, 1082
- Esposito, P., et al. 2007, *A&A* 476, 321
- Fernandez, R., & Thompson, C., 2007, *ApJ*, 660, 615
- Gavriil, F.P. & Kaspi, V.M. 2002, *ApJ*, 567, 1067
- Gavriil, F.P., Kaspi V.M., & Woods, P.M. 2002, *Nature*, 419, 142
- Gavriil, F.P. & Kaspi, V.M. 2004, *ApJ*, 609, L67
- Gavriil, Fotis P., Kaspi, V. M., & Woods, P. M. 2006, *ApJ*, 641, 418
- Gelfand, J. D. & Gaensler, B. M., 2007, *ApJ*, 667, 1111
- Goldreich, P. & Julian W.H. 1969, *ApJ*, 157, 869
- Gonzalez, M. E., Dib, R., Kaspi, V. M., Woods, P. M., Tam, C. R., Gavriil, F. P 2007, *ApJ* submitted (arXiv0708.2756)
- Götz, D., Mereghetti, S., Tiengo, A., Esposito, P. 2006, *A&A*, 449, L31
- Götz, D., et al. 2007, *A&A*, 475, 317
- Gotthelf, E. V.; Halpern, J. P.; Buxton, M.; Bailyn, C, 2004, *ApJ*, 605, 368
- Güver, T., Özel, F., Göğüs, E., Kouveliotou, C., 2007a, *ApJ*, 667, L73
- Güver, T., Özel, F., & Göğüs, 2007b, *ApJ* in press (arXiv0705.3982)
- Haberl, F., Freyberg, M. J., Briel, U. G., Dennerl, K., Zavlin, V. E. 2004, *SPIE*, 5165, 104

- Haberl, F., Zavlin, V.E., Trumper, J. & Burwitz, V., 2004, *A&A* 419, 1077
- Haberl, F. 2007, *Ap&SS*, 308, 73
- Halpern, J. P., Gotthelf, E. V., Reynolds, J., Ransom, S. M., Camilo, F., 2007, *ApJ* in press (arXiv0711.3780)
- Ho, W.C.G. & Lai, D. 2003, *MNRAS*, 338, 233
- Hulleman, F., van Kerkwijk, M.H. & Kulkarni, S.R. 2000, *Nature*, 408, 689
- Hurley, K., et al. 2005, *Nature*, 434, 1098
- Ibrahim, A. I., et al. 2004, *ApJ*, 609, L21
- Israel, G. L., Götz, D., Zane, S., Dall’Osso, S., Rea, N., Stella, L. 2007a, *A&A*, 476, L9I
- Israel, G. L., Campana, S., Dall’Osso, S., Munro, M. P., Cummings, J., Perna, R., Stella, L. 2007b, *ApJ*, 664, 448
- Jansen, F., et al. 2001, *A&A*, 365, L1
- Kaspi, V.M., Gavriil, F.P., Woods, P.M., Jensen, J.B., Roberts, M.S.E., & Chakrabarty, D., 2003, *ApJ*, 588, L93
- Kuiper, L., Hermsen, W., & Méndez, M. 2004, *ApJ*, 613, 1173
- Kuiper, L., Hermsen, W., den Hartog, P. R., Collmar, W., 2006, *ApJ*, 645, 556
- Lyutikov, M., & Gavriil F.P., 2006, *MNRAS*, 368, 690
- Lebrun, F., Leray, J.P., Lavocat, P., et al. 2003, *A&A*, 411, L141
- Lodders, K. 2003, *ApJ*, 591, 1220
- McLaughlin, M. A., et al. 2006, *Nature*, 439, 817
- Marsden, D. & White, N. E. 2001, *ApJ*, 551, L155
- Mereghetti, S., Tiengo, A., Stella, L., Israel, G.L., Rea, N., Zane, S., & Oosterbroek, T., 2004, *ApJ*, 608, 427
- Mereghetti, S., et al. 2005, *ApJ*, 628, 938
- Mereghetti, S., Götz, D., Mirabel, I. F., Hurley, K. 2005, *A&A* 433, L9

- Molkov, S., Hurley, K., Sunyaev, R., et al., 2005, *A&A*, 433, L13
- Muno, M. P., Gaensler, B. M., Clark, J. S., de Grijs, R., Pooley, D., Stevens, I. R., Portegies Zwart, S. F 2007, *MNRAS*, 378, L44
- Nobili, L., Turolla, R. & Zampieri, L. 1993, *ApJ*, 404, 686
- Palmer, D. M., et al. 2005, *Nature*, 434, 1107
- Perna, R., Heyl, J., Hernquist, L., 2000, *ApJ*, 541, 344
- Rea, N., et al. 2005, *MNRAS*, 361, 710
- Rea, N., Turolla, R., Zane, S., Tramacere, A., Israel, G.L., Stella, L., Campana, R., 2007a, *ApJ*, 661, L65
- Rea, N., Zane, S., Lyutikov, M. & Turolla, R., 2007b, *Ap&SS*, 308, 61
- Rea, N., et al. 2007c, *MNRAS*, 381, 293
- Strüder, L. et al. 2001, *A&A*, 365, L18
- Tam, C. R., Gavriil, F., Dib, R., Kaspi, V. M.; Woods, P. M., Bassa, C. 2007, *ApJ* in press (arXiv0707.2093)
- Thompson, C., & Beloborodov, A. M., *ApJ* 634, 565 (2005)
- Thompson, C., & Duncan, R.C., 1993, *ApJ*, 408, 194
- Thompson, C., & Duncan, R.C. 1995, *MNRAS*, 275, 255
- Thompson, C., & Duncan, R.C. 1996, *ApJ*, 473, 322
- Thompson, C., Lyutikov, M. & Kulkarni, S.R., 2002, *ApJ*, 574, 332
- Turner, M. J. L. et al. 2001, *A&A*, 365, L27
- Turolla, R., Zane, S. & Drake, J.J. 2004, *ApJ*, 603, 265
- Ubertini, P., et al. 2003, *A&A* 411, L131
- van Adelsberg, M. & Lai, D. 2006, *MNRAS*, 373, 1495
- van Paradijs, J., Taam, R.E., & van den Heuvel, E.P.J., 1995, *A&A*, 299, L41
- Woods, P.M., et al. 2004, *ApJ*, 605, 378

Woods, P.M., et al. 2005, ApJ, 629, 985

Woods, P. & Thompson, C., 2006, "Compact Stellar X-ray Sources", eds. W. H. G. Lewin
& M. van der Klis, 547

Table 1: Log Of The *XMM-Newton* and *INTEGRAL* Observations Analysed In This Paper.

<i>XMM-Newton</i>		
Source	Date (YYYY/MM/DD)	Exposure (ks)
4U 0142+614	2004/03/01	44
1RXS J1708-4009	2003/08/28	45
1E 1841-045	2002/10/07	6
1E 2259+586	2002/06/11	52
1E 1048-5937	2003/06/16	69
	2005/06/17	32
	2007/06/14	48
XTE J1810-197	2004/09/18	28
	2005/09/20	42
	2006/03/13	51
1E 1547.0-5408	2006/08/21	47
	2007/08/09	16
CXOU J1647-4552	2006/09/16	80
	2006/09/22	20
SGR 1806-20	2003/04/03	55
	2004/10/06	19
	2005/10/04	33
SGR 1900+14	2005/09/17	30
<i>INTEGRAL</i>		
Source	Date (YYYY/MM/DD)	Exposure (Ms)
4U 0142+614	2003/03/03-2006/08/13	1.9
1RXS J1708-4009	2003/02/28-2005/10/02	2.7
1E 1841-045	2003/03/10-2006/04/28	4.0
SGR 1900+14	2003/03/06-2006/09/26	3.7

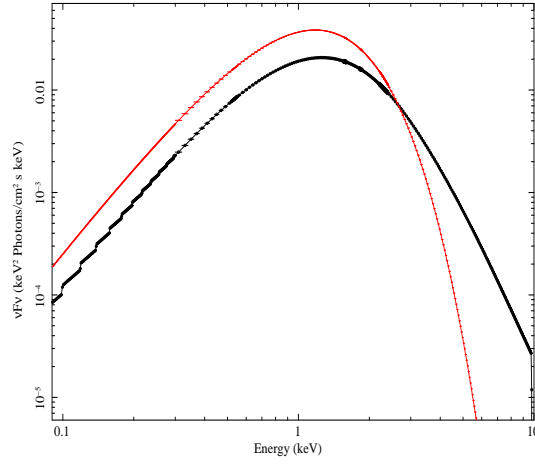


Fig. 1.— Thin red line shows a Plankian spectrum, represented here by an **XSPEC** blackbody model with temperature $kT=0.3$ keV (and 0.001 normalization), while the black thick line shows the same Plankian spectrum modified by the resonant cyclotron scattering. The RCS model here have parameters $\tau_{res} = 1$, $\beta_T=0.3$ and $T=0.3$ keV (and a normalization of 0.001).

Table 2: Spectral Parameters: 4U 0142+614, 1RXS J1708-4009, and 1E 1841-045

<i>AXPs</i>	4U 0142+614*		1RXS J1708-4009*		1E 1841-045	
Parameters	BB+2PL	RCS+PL	BB+2PL	RCS+PL	BB+PL	RCS+PL
N_H	$1.67^{+0.02}_{-0.02}$	$0.76^{+0.02}_{-0.02}$	$1.91^{+0.06}_{-0.06}$	$1.61^{+0.04}_{-0.04}$	$2.38^{+0.4}_{-0.1}$	$1.79^{+0.13}_{-0.15}$
constant	1.02	0.66	1.0	0.67	1.0	0.98
kT (keV)	$0.43^{+0.03}_{-0.03}$	$0.33^{+0.02}_{-0.02}$	$0.47^{+0.01}_{-0.01}$	$0.36^{+0.03}_{-0.02}$	$0.51^{+0.03}_{-0.02}$	$0.36^{+0.02}_{-0.02}$
BB norm	$8.7^{+0.4}_{-0.5} \times 10^{-4}$		$2.4^{+0.1}_{-0.2} \times 10^{-4}$		$2.4^{+0.6}_{-0.3} \times 10^{-4}$	
Γ_1	$4.14^{+0.04}_{-0.04}$		$2.70^{+0.08}_{-0.08}$			
PL ₁ norm	$0.30^{+0.08}_{-0.08}$		$0.016^{+0.003}_{-0.004}$			
β_T		$0.21^{+0.02}_{-0.02}$		$0.49^{+0.01}_{-0.01}$		$0.23^{+0.05}_{-0.05}$
τ_{res}		$1.7^{+0.2}_{-0.2}$		$1.2^{+0.2}_{-0.2}$		$1.6^{+0.4}_{-0.2}$
RCS norm		$0.016^{+0.01}_{-0.008}$		$8.0^{+1.1}_{-1.3} \times 10^{-4}$		$9.3^{+2.3}_{-1.1} \times 10^{-4}$
Γ_2	$0.78^{+0.1}_{-0.07}$	$1.0^{+0.1}_{-0.1}$	$0.76^{+0.1}_{-0.1}$	$0.8^{+0.1}_{-0.1}$	$1.47^{+0.04}_{-0.05}$	$1.45^{+0.06}_{-0.05}$
PL ₂ norm	$1.4^{+0.1}_{-0.1} \times 10^{-4}$	$7.7^{+0.1}_{-0.1} \times 10^{-4}$	$8.6^{+0.1}_{-0.1} \times 10^{-5}$	$2.6^{+0.1}_{-0.1} \times 10^{-4}$	$2.44^{+0.6}_{-0.6} \times 10^{-3}$	$2.1^{+0.1}_{-0.1} \times 10^{-3}$
Flux 1–10 keV	$1.1^{+0.8}_{-0.8} \times 10^{-10}$	$1.1^{+0.8}_{-0.8} \times 10^{-10}$	$2.6^{+0.3}_{-0.3} \times 10^{-11}$	$2.6^{+1.1}_{-0.8} \times 10^{-11}$	$2.2^{+0.2}_{-0.3} \times 10^{-11}$	$2.1^{+0.2}_{-0.3} \times 10^{-11}$
Flux 1–200 keV	$2.3^{+1.7}_{-1.1} \times 10^{-10}$	$2.7^{+1.0}_{-1.3} \times 10^{-10}$	$1.1^{+0.5}_{-0.5} \times 10^{-10}$	$1.4^{+0.8}_{-0.8} \times 10^{-10}$	$1.1^{+0.8}_{-0.8} \times 10^{-10}$	$1.1^{+0.8}_{-0.6} \times 10^{-10}$
χ^2_ν (dof)	0.99 (216)	1.19 (216)	1.11 (202)	1.09 (202)	1.14 (158)	1.12 (156)

Note. — Best fit values of the spectral parameters obtained by fitting the ~ 1 –200 keV *XMM-Newton* and *INTEGRAL* AXPs’ spectra with a blackbody plus two power-laws model (BB+2PL) for 4U 0142+614 and 1RXS J1708-4009, while a single power-law was used for 1E 1841-045. Furthermore, all the sources were modeled with a resonant cyclotron scattering model plus a power-law (RCS+PL). Errors are at 1σ confidence level, reported fluxes are absorbed and in units of $\text{ergs}^{-1}\text{cm}^{-2}$, and N_H in units of 10^{22}cm^{-2} and assuming solar abundances from Lodders (2003). See also Fig. 2 and § 4.1 for details. *: source slightly variable in flux and spectrum, see text for details.

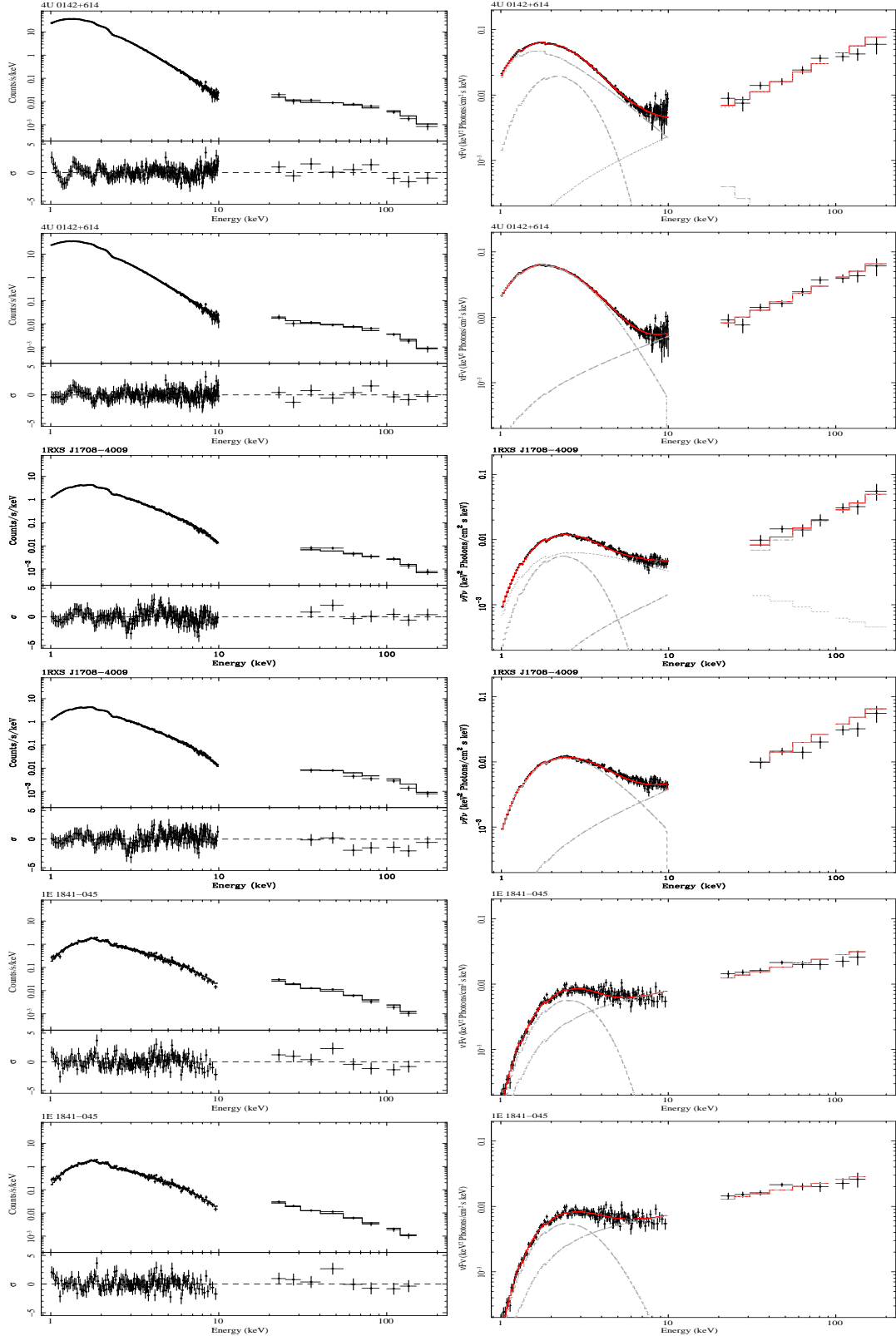


Fig. 2.— 4U 0142+614, 1RXS J1708-4009 and 1E 1841-045: left column shows the spectra in Count/s/keV while in the right column we report the $\nu F\nu$ plots. For 4U 0142+614 and 1RXS J1708-4009 the upper panels are relative to the modeling with a blackbody plus two power-laws (BB+2PL), while we used a blackbody plus power-law for 1E 1841-045. Bottom

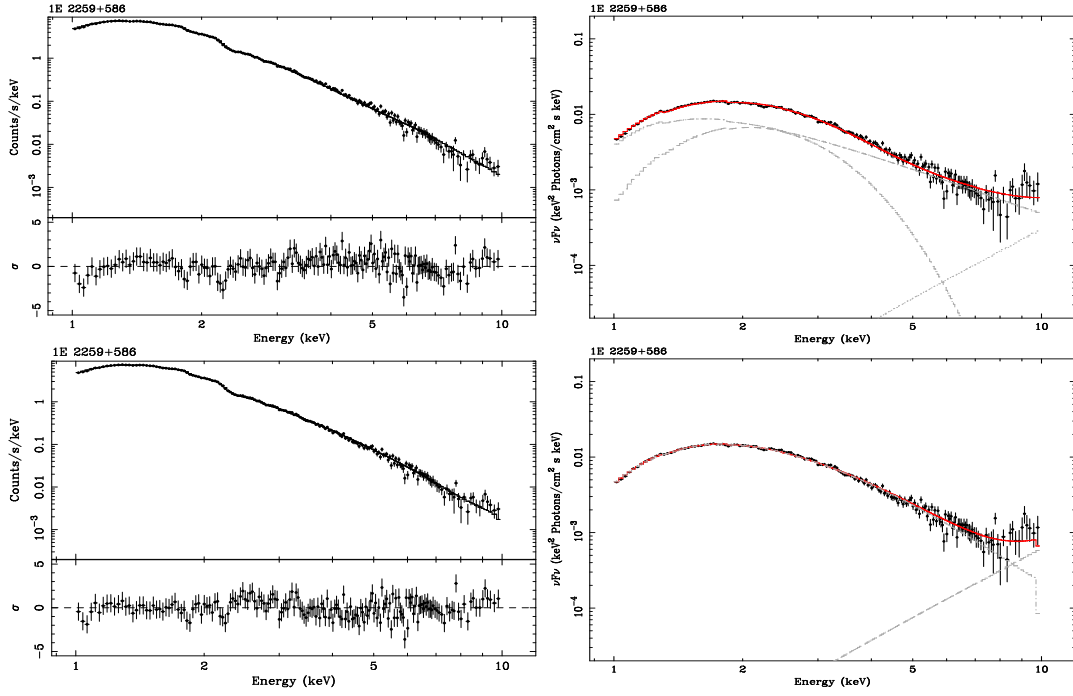


Fig. 3.— 1E 2259+586: left column shows the spectra in Count/s/keV while in the right column we report the $\nu F\nu$ plots. The upper panels are relative to the modeling with a blackbody plus two power-laws (BB+2PL), while bottom panels report the resonant cyclotron scattering plus a power-law model (RCS+PL). Note the hard X-ray spectrum has been fixed at the value from Kuiper et al. (2006). See Tab. 3 and § 4.1 for details.

Table 3: Spectral Parameters: 1E 2259+586

<i>AXP</i>	1E 2259+586*	
Parameters	BB+2PL	RCS+PL
N_H	$0.97^{+0.04}_{-0.03}$	$0.60^{+0.01}_{-0.02}$
kT (keV)	$0.41^{+0.03}_{-0.03}$	$0.31^{+0.02}_{-0.02}$
BB norm	$2.77^{+0.02}_{-0.01} \times 10^{-4}$	
Γ_1	$3.98^{+0.03}_{-0.02}$	
PL ₁ norm	$4.89^{+0.04}_{-0.04} \times 10^{-2}$	
β_T		$0.39^{+0.01}_{-0.01}$
τ_{res}		$1.64^{+0.02}_{-0.02}$
RCS norm		$0.31^{+0.04}_{-0.05} \times 10^{-4}$
Γ_2	1.02	1.02
PL ₂ norm	$1.65^{+1.0}_{-1.0} \times 10^{-7}$	$4.8^{+1.0}_{-1.0} \times 10^{-7}$
Flux 1–10 keV	$2.5^{+0.1}_{-0.1} \times 10^{-11}$	$2.5^{+0.1}_{-0.1} \times 10^{-11}$
χ^2_ν (dof)	1.15 (178)	1.12 (178)

Note. — Best fit values of the spectral parameters obtained by fitting the ~ 1 –10 keV *XMM-Newton* observation of 1E 2259+586 with a blackbody plus two power-laws model (BB+2PL), and with a resonant cyclotron scattering model plus a power-law (RCS+PL). We fixed the second power-law photon index to $\Gamma_2 = 1.02$, the value reported in Kuiper et al. (2006) from *RXTE* measurements. Errors are at 1σ confidence level, reported fluxes are absorbed and in units of $\text{erg s}^{-1}\text{cm}^{-2}$, and N_H in units of 10^{22} cm^{-2} and assuming solar abundances from Lodders (2003). See also Fig. 3 and § 4.1 for details. *: source variable in flux and spectrum, see text for details.

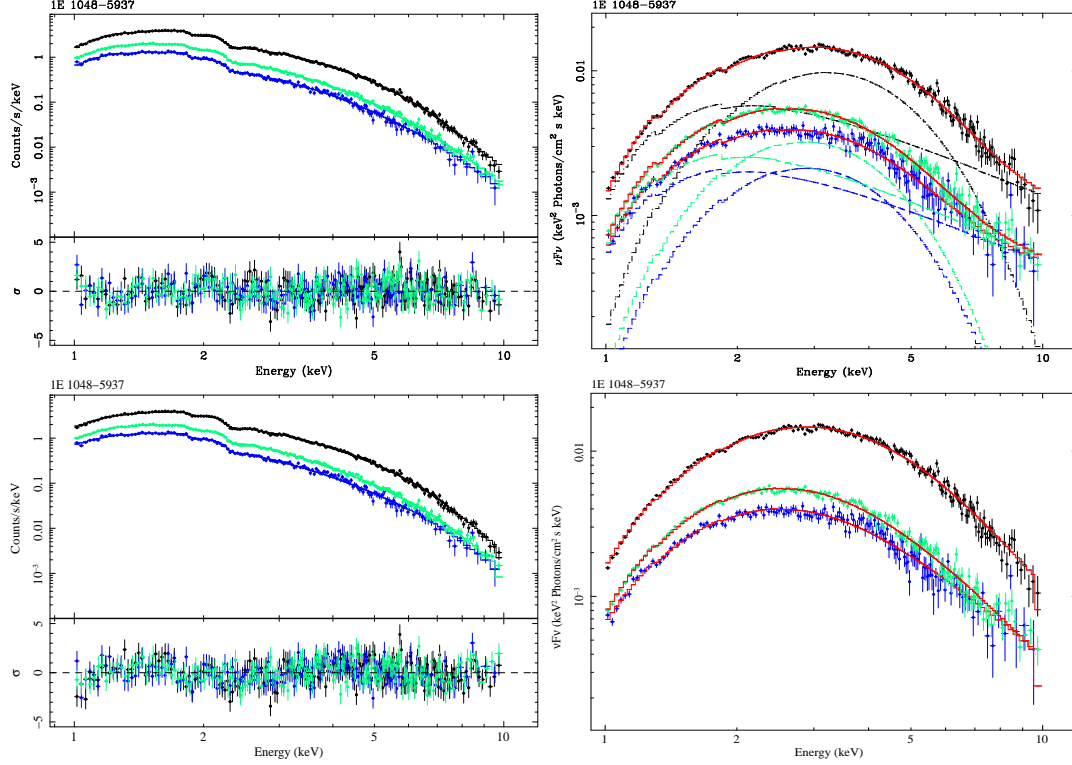


Fig. 4.— 1E 1048-5937: left column represents the spectra in Count/s/keV while in the right column we report the $\nu F\nu$ plots. The upper panels are relative to the modeling with a blackbody plus one power-law (BB+PL), while bottom panels report the resonant cyclotron scattering model (RCS). See Tab. 6 and § 4.2 for details. Black, blue, and light-green colors are relative to observations taken in 2007, 2005 and 2003, respectively. The red lines represent the total model, while the dashed lines are the single components.

Table 4: Spectral Parameters: 1E 1048-5937

<i>AXP</i>	1E 1048-5937					
	2003		2005		2007	
Parameters	BB+PL	RCS	BB+PL	RCS	BB+PL	RCS
N_H	$1.68^{+0.03}_{-0.03}$	$0.77^{+0.01}_{-0.02}$	$1.56^{+0.05}_{-0.04}$	$0.66^{+0.08}_{-0.07}$	$1.71^{+0.04}_{-0.03}$	$0.70^{+0.05}_{-0.05}$
kT (keV)	$0.63^{+0.02}_{-0.02}$	$0.52^{+0.01}_{-0.01}$	$0.64^{+0.03}_{-0.04}$	$0.52^{+0.02}_{-0.03}$	$0.73^{+0.01}_{-0.01}$	$0.61^{+0.03}_{-0.02}$
BB norm	$1.01^{+0.05}_{-0.05} \times 10^{-4}$		$0.7^{+0.1}_{-0.1} \times 10^{-4}$		$3.00^{+0.08}_{-0.08} \times 10^{-4}$	
Γ_1	$3.31^{+0.02}_{-0.04}$		$3.18^{+0.03}_{-0.04}$		$3.20^{+0.07}_{-0.07}$	
PL ₁ norm	$1.1^{+0.13}_{-0.04} \times 10^{-2}$		$0.7^{+0.1}_{-0.2} \times 10^{-2}$		$2.2^{+0.1}_{-0.1} \times 10^{-2}$	
β_T		$0.42^{+0.01}_{-0.02}$		$0.50^{+0.02}_{-0.02}$		$0.41^{+0.05}_{-0.04}$
τ_{res}		$1.99^{+0.06}_{-0.06}$		$1.81^{+0.05}_{-0.06}$		$1.98^{+0.04}_{-0.05}$
RCS norm		$0.20^{+0.05}_{-0.09}$		$4.08^{+0.08}_{-0.1} \times 10^{-4}$		$1.24^{+0.08}_{-0.1} \times 10^{-2}$
Flux 1–10 keV	$1.1^{+0.1}_{-0.1} \times 10^{-11}$	$1.1^{+0.1}_{-0.1} \times 10^{-11}$	$0.83^{+0.07}_{-0.08} \times 10^{-11}$	$0.83^{+0.07}_{-0.07} \times 10^{-11}$	$3.0^{+0.1}_{-0.1} \times 10^{-11}$	$3.0^{+0.1}_{-0.1} \times 10^{-11}$
χ^2_ν (dof)	0.99 (176)	1.08 (176)	0.99 (153)	1.050 (153)	1.08 (184)	1.29 (184)

Note. — Best fit values of the spectral parameters obtained by fitting several ~ 1 –10 keV *XMM-Newton* spectra, taken in different source states, with a blackbody plus power-law model (BB+PL), and with a resonant cyclotron scattering model (RCS). Errors are at 1σ confidence level, reported fluxes are absorbed and in units of $\text{ergs}^{-1}\text{cm}^{-2}$, and N_H in units of 10^{22}cm^{-2} and assuming solar abundances from Lodders (2003). See also Fig. 4 and § 4.2 for details.

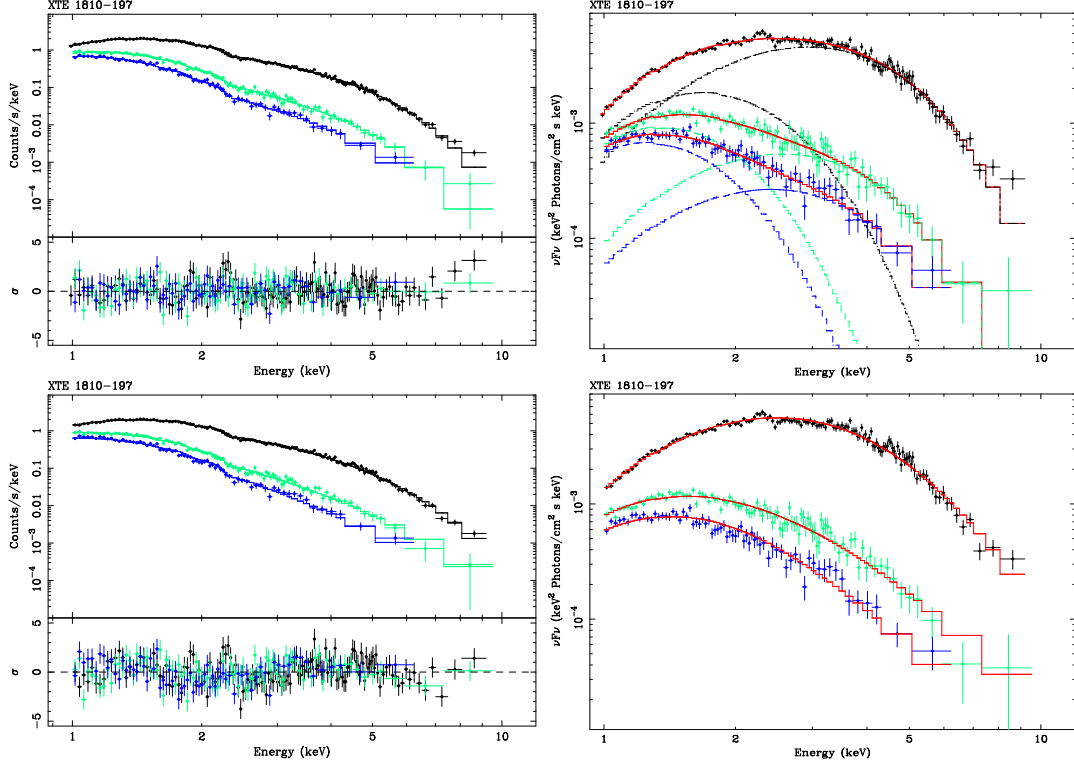


Fig. 5.— XTE J1810-197: left column represents the spectra in Count/s/keV while in the right column we report the $\nu F\nu$ plots. The upper panels are relative to the modeling with two absorbed blackbodies (BB+BB), while bottom panels report the resonant cyclotron scattering model (RCS). See also Tab.6 and § 4.2 for details. Black, light-green and blue colors are relative to observations taken on 2004, 2005 and 2006, respectively. The red lines represent the total model, while the dashed lines are the single components.

Table 5: Spectral Parameters: XTE J1810-197

<i>AXP</i>	XTE J1810-197					
	2004		2005		2006	
Parameters	BB+BB	RCS	BB+BB	RCS	BB+BB	RCS
N_H	$0.58^{+0.06}_{-0.05}$	$0.35^{+0.08}_{-0.1}$	$0.52^{+0.08}_{-0.07}$	$0.22^{+0.5}_{-0.4}$	$0.4^{+0.1}_{-0.1}$	$0.2^{+0.1}_{-0.1}$
kT_1 (keV)	$0.36^{+0.02}_{-0.02}$	$0.56^{+0.03}_{-0.03}$	$0.27^{+0.03}_{-0.02}$	$0.32^{+0.08}_{-0.07}$	$0.25^{+0.03}_{-0.04}$	$0.3^{+0.1}_{-0.1}$
BB ₁ norm	$6.6^{+0.5}_{-0.4} \times 10^{-5}$		$3.8^{+0.2}_{-0.1} \times 10^{-5}$		$2.7^{+0.3}_{-0.3} \times 10^{-5}$	
kT_2 (keV)	$0.71^{+0.01}_{-0.02}$		$0.58^{+0.03}_{-0.03}$		$0.36^{+0.05}_{-0.07}$	
BB ₂ norm	$12^{+1}_{-1} \times 10^{-5}$		$1.5^{+0.1}_{-0.1} \times 10^{-5}$		$0.7^{+0.1}_{-0.1} \times 10^{-5}$	
β_T		$0.21^{+0.07}_{-0.05}$		$0.38^{+0.08}_{-0.08}$		$0.4^{+0.1}_{-0.1}$
τ_{res}		$1.08^{+0.04}_{-0.05}$		$1.02^{+0.06}_{-0.06}$		$1.46^{+0.08}_{-0.1}$
RCS norm		$9.3^{+0.3}_{-0.3} \times 10^{-5}$		$7.1^{+0.3}_{-0.4} \times 10^{-5}$		$7.5^{+0.5}_{-0.5} \times 10^{-5}$
Flux 1–10 keV	$12^{+3}_{-2} \times 10^{-12}$	$11^{+3}_{-3} \times 10^{-12}$	$2.2^{+0.1}_{-0.2} \times 10^{-12}$	$2.1^{+0.2}_{-0.2} \times 10^{-12}$	$1.2^{+0.3}_{-0.4} \times 10^{-12}$	$1.2^{+0.5}_{-0.4} \times 10^{-12}$
χ^2_ν (dof)	1.21 (135)	1.25 (135)	0.94 (97)	1.08 (97)	0.97 (67)	1.10 (67)

Note. — Best fit values of the spectral parameters obtained by fitting several ~ 1 –10 keV *XMM-Newton* spectra, taken in different source states, with two absorbed blackbodies (BB+BB), and with a resonant cyclotron scattering model (RCS). Errors are at 1σ confidence level, reported fluxes are absorbed and in units of $\text{erg s}^{-1} \text{cm}^{-2}$, and N_H in units of 10^{22}cm^{-2} and assuming solar abundances from Lodders (2003). See also Fig. 5 and § 4.2 for details.

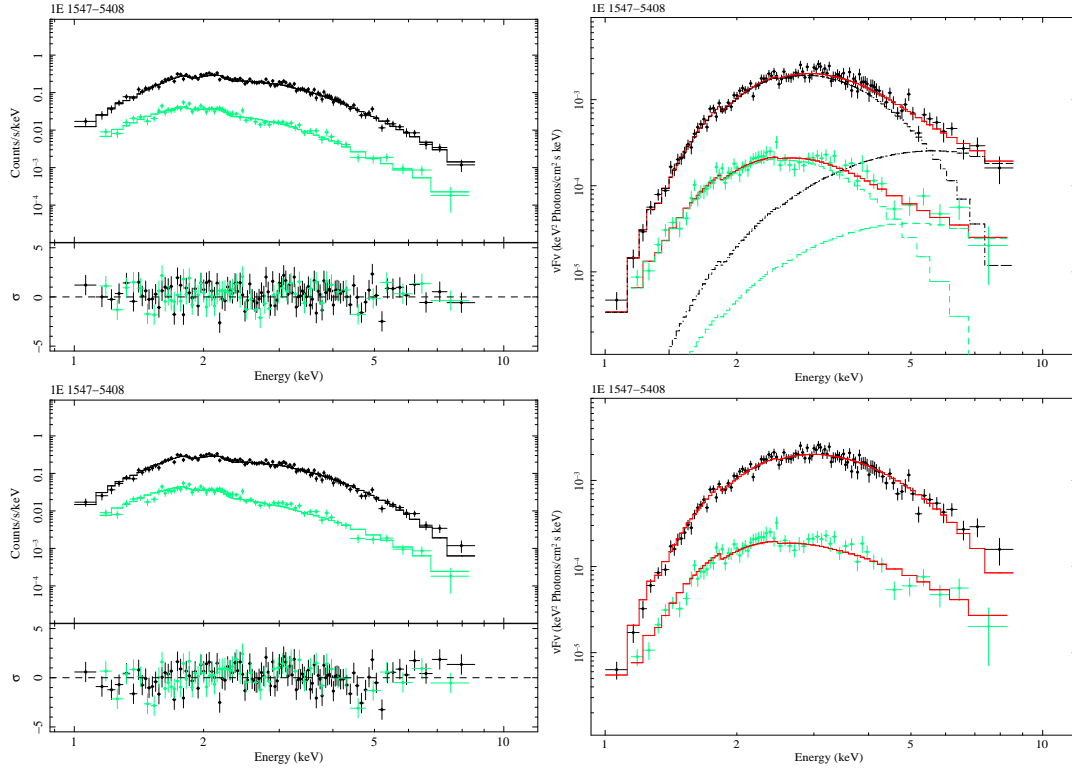


Fig. 6.— 1E 1547.0-5408: left column represents the spectra in Count/s/keV while in the right column we report the νF_ν plots. The upper panels are relative to the modeling with two blackbodies (BB+BB), while bottom panels report the resonant cyclotron scattering model (RCS). See also Tab. 6 and § 4.2 for details. Black and light-green colors are relative to observations taken on 2007 and 2006, respectively. The red lines represent the total model, while the dashed lines are the single components.

Table 6: Spectral Parameters: 1E 1547.0-5408

<i>AXP</i>	1E 1547.0-5408			
	2006		2007	
Parameters	BB+BB	RCS	BB+BB	RCS
N_H	$3.76^{+0.06}_{-0.05}$	$4.1^{+0.1}_{-0.1}$	$4.58^{+0.08}_{-0.07}$	$4.0^{+0.1}_{-0.1}$
kT_1 (keV)	$0.46^{+0.03}_{-0.02}$	$0.30^{+0.06}_{-0.06}$	$0.51^{+0.02}_{-0.02}$	$0.52^{+0.08}_{-0.07}$
BB ₁ norm	$1.2^{+0.5}_{-0.4} \times 10^{-5}$		$7.2^{+0.5}_{-0.5} \times 10^{-6}$	
kT_2 (keV)	$1.2^{+0.1}_{-0.1}$		$1.34^{+0.08}_{-0.07}$	
BB ₂ norm	$1.4^{+0.1}_{-0.1} \times 10^{-6}$		$1.4^{+0.1}_{-0.1} \times 10^{-4}$	
β_T		$0.47^{+0.07}_{-0.05}$		$0.14^{+0.04}_{-0.05}$
τ_{res}		$1.07^{+0.04}_{-0.05}$		$1.33^{+0.06}_{-0.06}$
RCS norm		$4.2^{+0.3}_{-0.3} \times 10^{-5}$		$7.2^{+0.3}_{-0.4} \times 10^{-5}$
Flux 1–10 keV	$3.2^{+0.1}_{-0.1} \times 10^{-13}$	$3.1^{+0.1}_{-0.2} \times 10^{-13}$	$3.0^{+0.1}_{-0.1} \times 10^{-12}$	$3.0^{+0.2}_{-0.2} \times 10^{-12}$
χ^2_ν (dof)	1.18 (60)	1.07 (60)	1.02 (105)	1.08 (105)

Note. — Best fit values of the spectral parameters obtained by fitting several ~ 1 –10 keV *XMM-Newton* spectra, taken in different source states, with two absorbed blackbodies (BB+BB), and with a resonant cyclotron scattering model (RCS). Errors are at 1σ confidence level, reported fluxes are absorbed and in units of $\text{erg s}^{-1} \text{cm}^{-2}$, and N_H in units of 10^{22}cm^{-2} and assuming solar abundances from Lodders (2003). See also Fig. 6 and § 4.2 for details.

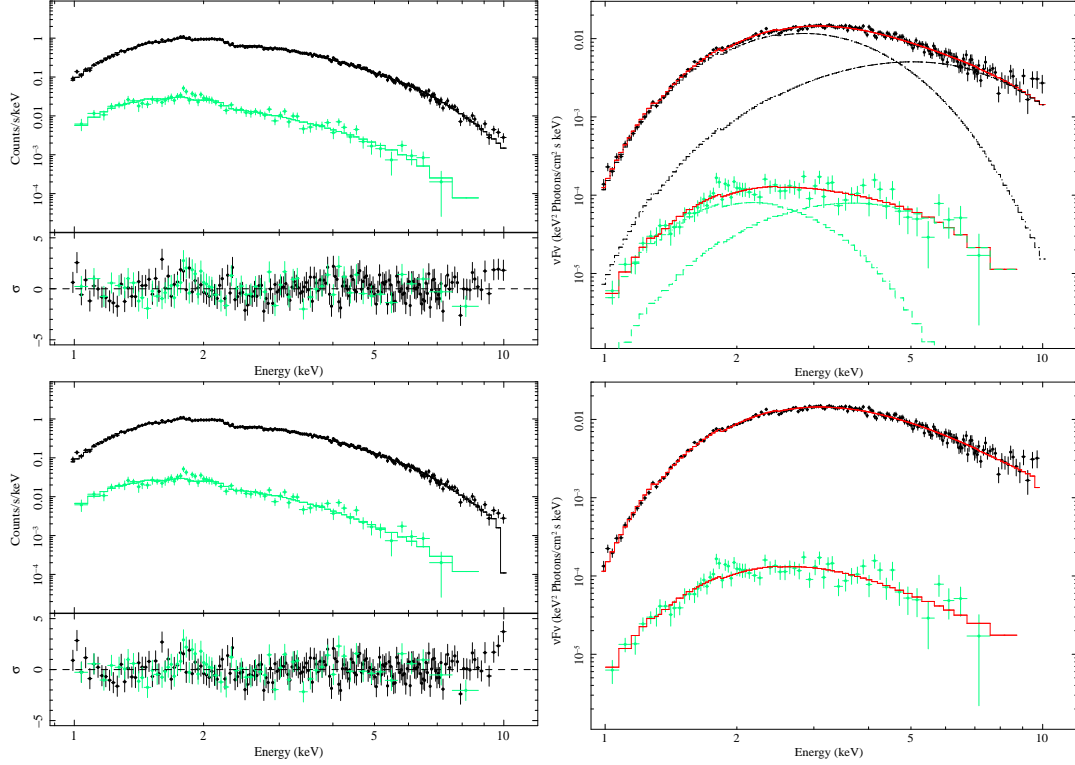


Fig. 7.— CXOU J1647-4552: left column represents the spectra in Count/s/keV while in the right column we report the $\nu F\nu$ plots. The upper panels are relative to the modeling with two absorbed blackbodies (BB+BB), while bottom panels report the resonant cyclotron scattering model (RCS). See also Tab. 7 and § 4.2 for details. Black and light-green colors are relative to observations taken on 2006 September 22 and 16, respectively. The red lines represent the total model, while the dashed lines are the single components.

Table 7: Spectral Parameters: CXOU J1647-4552

<i>AXP</i>	CXOU J1647-4552			
	2006/09/16		2006/09/22	
Parameters	BB+BB	RCS	BB+BB	RCS
N_H	$2.14^{+0.06}_{-0.06}$	$1.72^{+0.08}_{-0.1}$	$2.64^{+0.04}_{-0.04}$	$2.56^{+0.08}_{-0.08}$
kT_1 (keV)	$0.39^{+0.03}_{-0.02}$	$0.30^{+0.06}_{-0.06}$	$0.50^{+0.02}_{-0.02}$	$0.56^{+0.08}_{-0.07}$
BB ₁ norm	$4.5^{+0.5}_{-0.4} \times 10^{-6}$		$2.7^{+0.5}_{-0.5} \times 10^{-4}$	
kT_2 (keV)	$0.84^{+0.1}_{-0.1}$		$0.94^{+0.04}_{-0.04}$	
BB ₂ norm	$2.4^{+0.1}_{-0.1} \times 10^{-6}$		$2.5^{+0.1}_{-0.1} \times 10^{-4}$	
β_T		$0.21^{+0.07}_{-0.05}$		$0.48^{+0.08}_{-0.08}$
τ_{res}		$1.02^{+0.04}_{-0.05}$		$1.67^{+0.06}_{-0.06}$
RCS norm		$3.6^{+0.3}_{-0.3} \times 10^{-6}$		$7.2^{+0.3}_{-0.4} \times 10^{-4}$
Flux 1–10 keV	$2.4^{+0.1}_{-0.1} \times 10^{-13}$	$2.4^{+0.1}_{-0.1} \times 10^{-13}$	$2.2^{+0.1}_{-0.1} \times 10^{-11}$	$2.2^{+0.1}_{-0.1} \times 10^{-11}$
χ^2_ν (dof)	1.00 (73)	(73)	1.01 (136)	1.08 (136)

Note. — Best fit values of the spectral parameters obtained by fitting several ~ 1 –10 keV *XMM-Newton* spectra, taken in different source states, with two absorbed blackbodies (BB+BB), and with a resonant cyclotron scattering model (RCS). Errors are at 1σ confidence level, reported fluxes are absorbed and in units of $\text{erg s}^{-1} \text{cm}^{-2}$, and N_H in units of 10^{22}cm^{-2} and assuming solar abundances from Lodders (2003). See also Fig. 7 and § 4.2 for details.

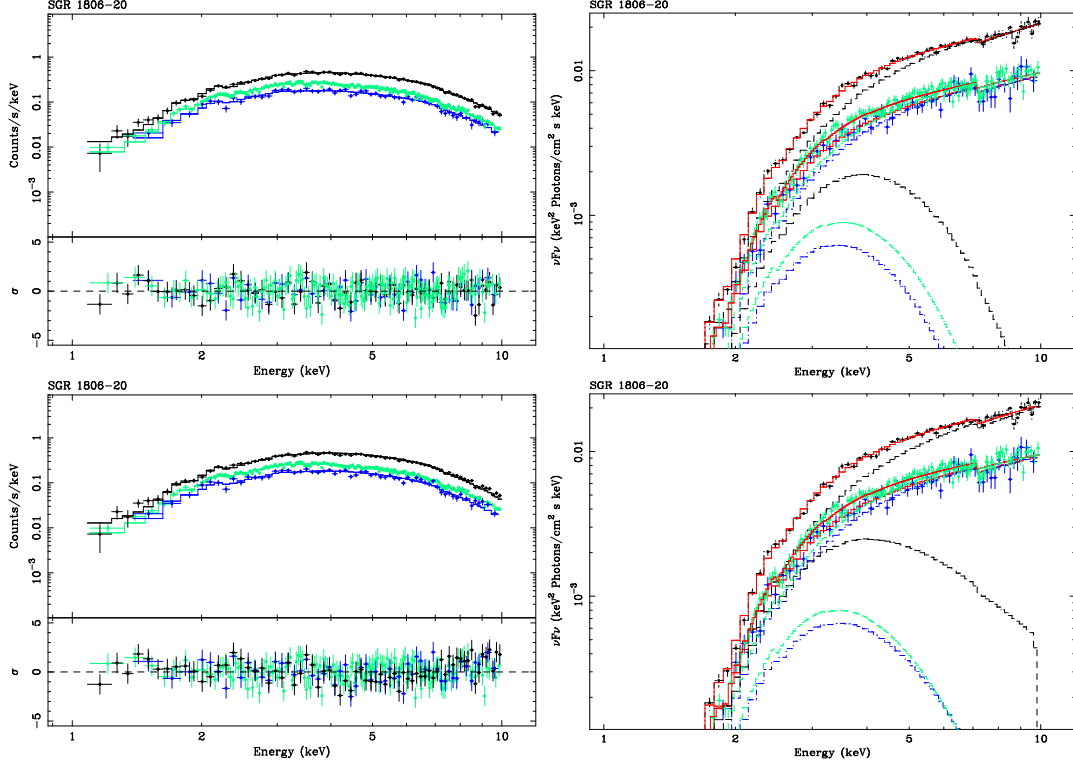


Fig. 8.— SGR1806-20: left column shows the spectra in Count/s/keV while in the right column we report the νF_ν plots. The upper panels are relative to the modeling with a blackbody plus power-law (BB+PL), while bottom panels report the resonant cyclotron scattering model plus power-law (RCS+PL). See also Tab.6 and §4.3 for details. Light green, black and blue colours are relative to observations taken on 2003, 2004 and 2005, respectively. The red lines represent the total model, while the dashed lines are the single components.

Table 8: Spectral Parameters: SGR 1806-20

<i>SGR</i>	SGR 1806-20					
	2003		2004		2005	
Parameters	BB+PL	RCS+PL	BB+PL	RCS+PL	BB+PL	RCS+PL
N_H	$9.9^{+0.4}_{-0.4}$	$9.9^{+1.0}_{-0.8}$	$9.7^{+0.2}_{-0.2}$	$10.2^{+0.6}_{-0.8}$	$10.2^{+1.0}_{-0.8}$	$10.4^{+1.0}_{-0.8}$
kT (keV)	$0.56^{+0.05}_{-0.04}$	$0.50^{+0.06}_{-0.1}$	$0.72^{+0.06}_{-0.07}$	$0.56^{+0.06}_{-0.05}$	$0.57^{+0.04}_{-0.04}$	$0.51^{+0.07}_{-0.08}$
BB norm	$5.5^{+0.3}_{-0.3} \times 10^{-5}$		$1.0^{+0.4}_{-0.3} \times 10^{-4}$		$7.4^{+0.4}_{-0.3} \times 10^{-5}$	
β_T		$0.11^{+0.03}_{-0.03}$		$0.45^{+0.03}_{-0.04}$		$0.10^{+0.04}_{-0.03}$
τ_{res}		$2.1^{+0.1}_{-0.1}$		$1.7^{+0.2}_{-0.3}$		$1.0^{+0.2}_{-0.3}$
RCS norm		$3.7^{+0.5}_{-0.5} \times 10^{-5}$		$2.7^{+0.7}_{-0.8} \times 10^{-4}$		$5.0^{+0.7}_{-0.8} \times 10^{-5}$
Γ	$1.5^{+0.1}_{-0.1}$	$1.5^{+0.1}_{-0.1}$	$1.3^{+0.1}_{-0.1}$	$1.2^{+0.1}_{-0.1}$	$1.5^{+0.1}_{-0.1}$	$1.6^{+0.2}_{-0.1}$
PL norm	$3.1^{+0.2}_{-0.2} \times 10^{-3}$	$3.1^{+0.2}_{-0.3} \times 10^{-3}$	$4.7^{+0.2}_{-0.2} \times 10^{-3}$	$4.1^{+0.4}_{-0.3} \times 10^{-3}$	$3.8^{+0.2}_{-0.3} \times 10^{-3}$	$4.3^{+0.8}_{-1.0} \times 10^{-3}$
Flux 1–10 keV	$1.2^{+0.5}_{-0.6} \times 10^{-11}$	$1.2^{+0.8}_{-0.8} \times 10^{-11}$	$2.6^{+0.6}_{-0.7} \times 10^{-11}$	$2.6^{+0.7}_{-0.8} \times 10^{-11}$	$1.4^{+0.5}_{-0.6} \times 10^{-11}$	$1.3^{+0.8}_{-0.8} \times 10^{-11}$
χ^2_ν (dof)	0.96 (54)	1.00 (52)	1.01 (65)	0.95 (63)	1.02 (159)	1.00 (157)

Note. — Best fit values of the spectral parameters obtained by fitting several ~ 1 –10 keV *XMM-Newton* spectra, taken in different source states, with a blackbody plus power-law model (BB+PL), and with a resonant cyclotron scattering plus power-law model (RCS+PL). Errors are at 1σ confidence level, reported fluxes are absorbed and in units of $\text{ergs}^{-1}\text{cm}^{-2}$, and N_H in units of 10^{22}cm^{-2} and assuming solar abundances from Lodders (2003). See also Fig. 8 and §4.3 for details.

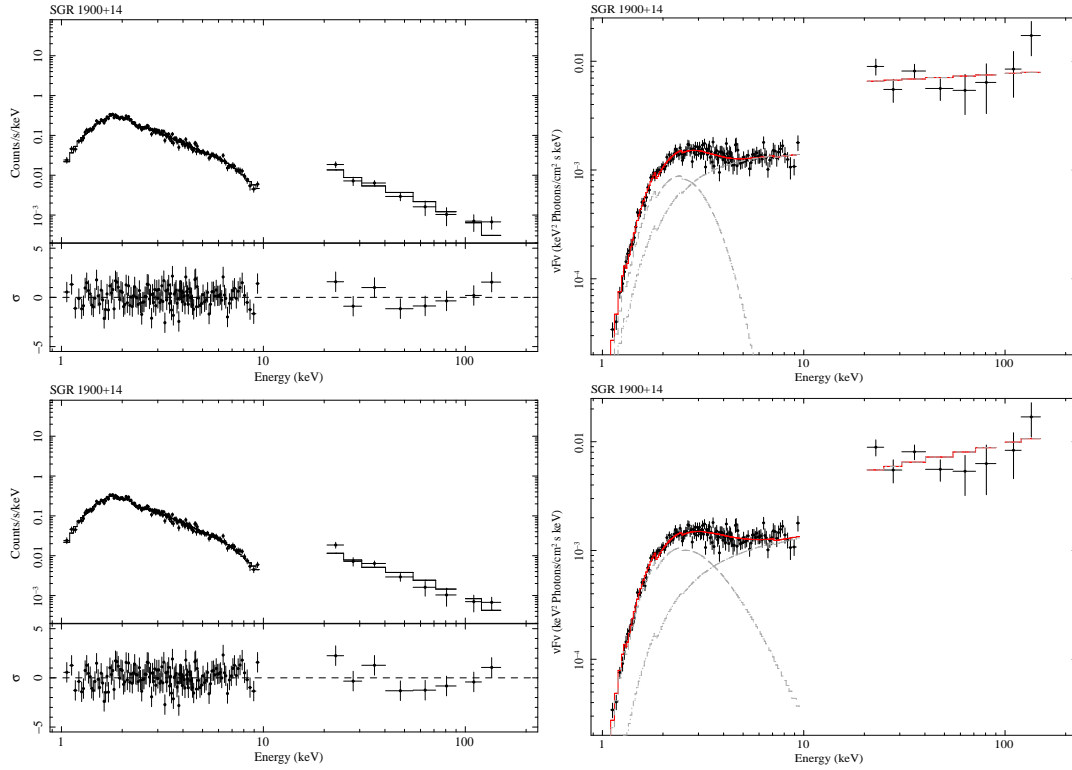


Fig. 9.— SGR 1900+14: left column shows the spectra in Count/s/keV while in the right column we report the $\nu F\nu$ plots. The upper panels are relative to the modeling with a blackbody plus power-law (BB+PL), while bottom panels report the resonant cyclotron scattering model plus power-law (RCS+PL). See also Tab.9 and §4.3 for details. The red lines represent the total model, while the dashed lines are the single components.

Table 9: Spectral Parameters: SGR 1900+14

<i>SGR</i>	SGR 1900+14	
Parameters	BB+PL	RCS+PL
N_H	$3.35^{+0.08}_{-0.08}$	$4.0^{+0.1}_{-0.1}$
constant	1.2	1.1
kT (keV)	$0.47^{+0.04}_{-0.03}$	$0.31^{+0.02}_{-0.02}$
BB norm	$5.2^{+0.1}_{-0.1} \times 10^{-5}$	
Γ	$1.6^{+0.1}_{-0.1}$	$1.6^{+0.1}_{-0.1}$
PL norm	$6.6^{+0.1}_{-0.1} \times 10^{-4}$	$5.9^{+0.1}_{-0.1} \times 10^{-4}$
β_T		$0.35^{+0.01}_{-0.01}$
τ_{res}		$1.28^{+0.02}_{-0.01}$
RCS norm		$2.4^{+0.04}_{-0.05} \times 10^{-4}$
Flux 1–10 keV	$3.9^{+0.1}_{-0.1} \times 10^{-12}$	$3.8^{+0.1}_{-0.1} \times 10^{-12}$
Flux 1–200 keV	$1.7^{+0.1}_{-0.1} \times 10^{-11}$	$1.7^{+0.1}_{-0.1} \times 10^{-11}$
χ^2_ν (dof)	1.12 (141)	1.18 (139)

Note. — Best fit values of the spectral parameters obtained by fitting the ~ 1 –200 keV *XMM-Newton* and *INTEGRAL* spectra with a blackbody plus a power-law model (BB+PL), and with a resonant cyclotron scattering model plus a power-law (RCS+PL). Errors are at 1σ confidence level, reported fluxes are absorbed and in units of $\text{ergs}^{-1}\text{cm}^{-2}$, and N_H in units of 10^{22}cm^{-2} and assuming solar abundances from Lodders (2003). See also Fig. 9 and §4.3 for details.

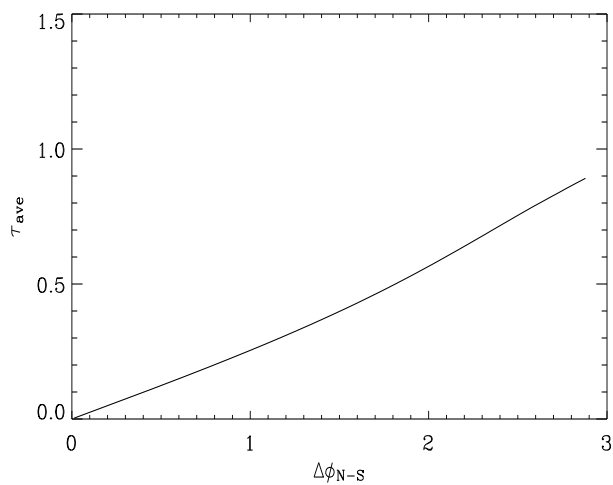


Fig. 10.— Angle-averaged optical depth in a twisted magnetosphere model (Thompson Lyutikov & Kulkarni 2002) as a function of the twist angle. The curve refers to $\beta_{bulk} = 1$; for different values of the bulk velocity the ordinate should be divided by β_{bulk} .

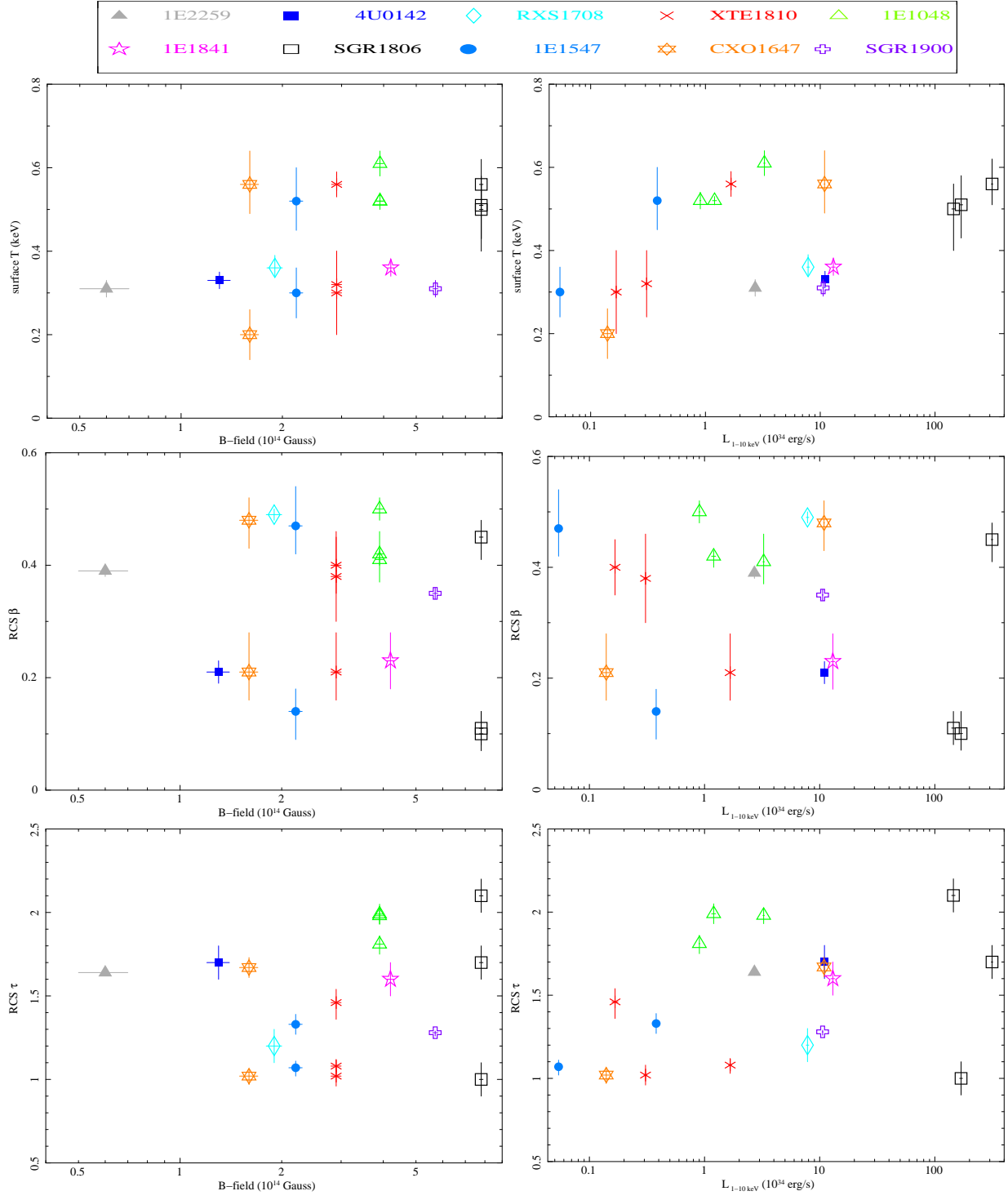


Fig. 11.— Comparison between the derived spectral parameters and the sources’ properties (see §5 for details).